Organic Geochemistry 173 (2022) 104504

Contents lists available at ScienceDirect

Organic Geochemistry

journal homepage: www.elsevier.com/locate/orggeochem

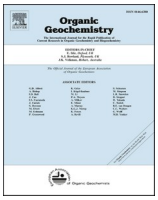

Exceptional molecular preservation in the Late Jurassic Claudia palaeo-geothermal field (Deseado Massif, Patagonia, Argentina)

Bronwyn L. Teece [a,*], Diego M. Guido [b], Kathleen A. Campbell [c], Martin J. Van Kranendonk [a], Amanda Galar [b], Simon C. George [d]

[a] Australian Centre for Astrobiology, School of Biological, Earth and Environmental Sciences, University of New South Wales, Sydney 2052, Australia
[b] CONICET and Facultad de Ciencias Naturales y Museo, Universidad Nacional de La Plata, Instituto de Recursos Minerales (INREMI), Calle 64 y 120, La Plata 1900, Argentina
[c] School of Environment and Te Ao Mārama – Centre of Fundamental Inquiry, Faculty of Science, The University of Auckland, Private Bag 92019, Auckland 1142, New Zealand
[d] School of Natural Sciences, Macquarie University, Sydney, NSW 2109, Australia

ARTICLE INFO

Associate Editor—**Kliti Grice**

Keywords:
Astrobiology
Biomarkers
Hydrocarbons
Hot spring

ABSTRACT

Gas chromatography–mass spectrometry was applied to samples collected from an exceptionally well-preserved Late Jurassic (~150 Ma) sinter complex of the Claudia palaeo-geothermal field, Deseado Massif geological province, Argentinean Patagonia, which, despite its age, has never been deeply buried. Results indicate that the distal sinter apron has a much higher preservation potential for indigenous organic matter (OM) than the more proximal (vent area) facies of this palaeo-geothermal field. Specifically, homohopane ratios show that the OM of the proximal apron is of mixed thermal maturities and is in low abundance. In contrast, the OM extracted from the distal apron contains highly abundant, thermally immature biomarkers, the presence of which are consistent with the lower original fluid temperatures of the distal spring facies. Moreover, despite indications of the presence of some thermally mature aromatic compounds, hopane and sterane ratios confirm that the distal apron samples are extremely thermally immature and thereby constitute an area of exceptional molecular preservation. From an astrobiological viewpoint, these results suggest that silica sinter can preserve abundant organics over millions of years in palaeoenvironmentally conducive settings, and that sample-site selection within a hot spring facies-model framework may be critical in the successful search for ancient extra-terrestrial life.

1. Introduction

Siliceous hot spring deposits, or sinters, are chemical sedimentary rocks that mainly form where near-neutral pH, alkali chloride thermal fluids discharge and cool at Earth's surface along a temperature gradient from proximal spring-vents (~100–70 °C), to moderate temperature (~65–40 °C) channels and pools of the middle sinter apron, to cooler (<40 °C) distal apron terraces, and into the surrounding, ambient (~25 °C) marsh (Walter, 1976; Cady and Farmer, 1996; Renaut and Jones, 2011). As the thermal spring fluids discharge downslope and laterally spread across substrates in geothermal fields, silica precipitates and commonly entraps indigenous organisms in situ, preserving an ecological record of the landscape at the time of deposition (Trewin et al., 1996; Jones et al., 1998; Channing and Edwards, 2009; Guido et al., 2010; Watts-Henwood et al., 2017; Hamilton et al., 2019; Campbell et al., 2020).

Research on biomarker preservation in modern sinters has been gaining more attention because of their potential preservation of robust geochemical biosignatures into the deep-time geological record (e.g., Hays et al., 2017), with potential applications to Mars (Ruff and Farmer, 2016). Importantly, sinter deposits are now known from almost the entire geological record on Earth, including the Paleoarchean (Djokic et al., 2017, 2021; Van Kranendonk et al., 2021), and Noachian opaline sinters have also been inferred from discoveries by the *Spirit* rover at Columbia Hills, Gusev Crater, Mars, and from orbital data from elsewhere on the planet (Squyres et al., 2008; Skok et al., 2010; Ruff and Farmer, 2016; Cady et al., 2018; Ruff et al., 2020).

In sinter aprons derived from alkali chloride hot-spring discharge, prokaryotes (including extremophile archaea) dominate the higher temperature portions, whereas cyanobacteria dominate the middle to

* Corresponding author.
E-mail address: b.teece@unsw.edu.au (B.L. Teece).

https://doi.org/10.1016/j.orggeochem.2022.104504
Received 22 May 2022; Received in revised form 8 September 2022; Accepted 11 September 2022
Available online 15 September 2022

distal apron portions, and eukaryotes flourish in distal apron margins to geothermally influenced marsh areas (Cady and Farmer, 1996; Renaut and Jones, 2011). Although the preservation potential of different types of environmentally indicative textures in discrete hot spring facies has been well documented (Cady and Farmer, 1996; Jones et al., 1998; Campbell et al., 2001, 2015; Jones et al., 2001; Guidry and Chafetz, 2003; Wilmeth et al., 2020, 2021; Djokic et al., 2021), the mechanisms that govern the preservation of hydrocarbons derived from the lipid membranes of prokaryotes and eukaryotes in sinters are less well understood.

In particular, hydrothermal fluids not only deposit primary silica from discharging spring sources at the Earth's surface, but repeated fluid pulses and shifts in fluid pH during the lifetimes of some hydrothermal systems may cause multiple phases of silicification, dissolution/reprecipitation, as well as diagenetic recrystallisation of the silica (e.g. Herdianita et al., 2000; Campbell et al., 2001, 2019; Lynne and Campbell, 2003; Rodgers et al., 2004; Lynne et al., 2005; Jones and Renaut, 2012). Primary organic matter (OM) may become entombed during early silicification, or decay and disappear through subsequent phases of weathering and/or hydrothermal alteration. Alternatively, primary OM may become buried and then entrained in the hydrothermal fluids to migrate through the system and be redistributed as secondary OM (Zundel and Rohmer, 1985; Gonsior et al., 2018; Campbell et al., 2019; Reinhardt et al., 2019; Teece et al., 2020). Therefore, the varied nature of hot spring depositional and post-depositional conditions translates to varied preservation potential of not only the different sedimentary facies in sinters, but also the quality of preservation of the affiliated OM.

Here, we further examine the hypothesis put forth by Williams et al. (2021) from Subrecent-active Icelandic hot springs that different facies from alkali chloride hot springs have different preservation potential for OM, controlled initially by the differential temperature gradient (~100 °C to ambient) of the discharging geothermal fluid as it cools during transport from the proximal source area to the distal edge of a sinter apron.

In the 40 km^2 Claudia palaeo-geothermal field, the focus of this study, the best preserved siliceous hot spring deposits, based on textural and petrographic observations, are at the Loma Alta and La Calandria Sur outcrop areas (Guido and Campbell, 2014; Guido et al., 2019). Our new molecular biomarker results from these outcrops, as delineated below, suggest that the distal marsh areas of the Claudia palaeo-hydrothermal system represent pristine molecular lagerstätte (cf. Allison, 1988), owing to the occurrence of immature steranes and hopanes. In comparison, the proximal sinter apron area at Claudia shows variability in the quality of molecular preservation. These results imply that the cooler margins of geothermally influenced depositional settings provide the best targets to search for abundant and thermally immature compounds in ancient hot spring environments.

2. Geological setting

The Late Jurassic Claudia palaeo-geothermal field in the Deseado Massif of Patagonia, Argentina records excellent biotic preservation within a ~150 m.y. old quartzose sinter, with minimal evidence of hydrothermal alteration in the analysed sinter apron areas, and minimal post-depositional burial. Based on previous petrographic and Raman analyses, the Claudia locality contains the best-preserved sinter deposit in the Deseado Massif (Guido and Campbell, 2011, 2014; Guido et al., 2019), but to date there have been no studies on the composition and quality of preservation of its OM content.

The Claudia palaeo-geothermal field (Fig. 1) comprises a group of hot spring deposits within the Deseado Massif, a 60,000 km^2 geological province located in Patagonia, southern Argentina. The Massif is

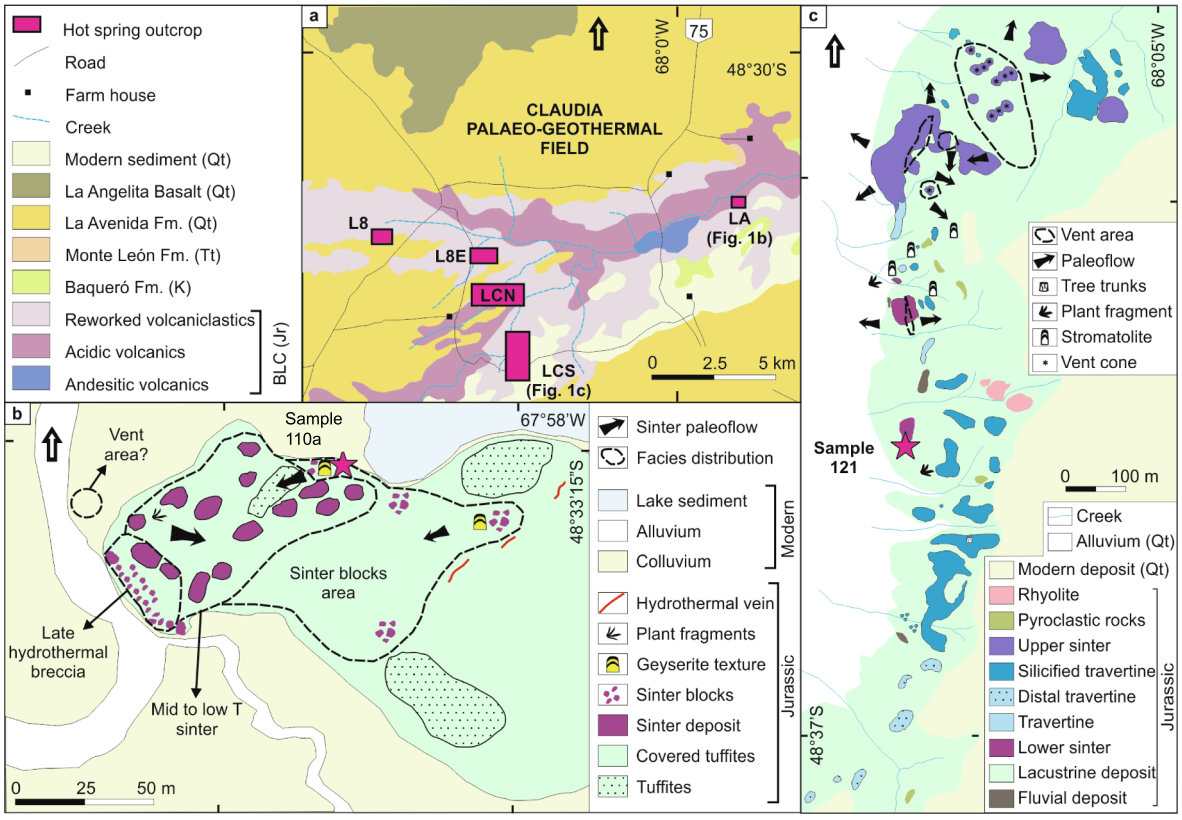

Fig. 1. (a) Regional geological map of the Claudia hot spring outcrops: LA = Loma Alta; L8 = Lote 8; L8E = Lote 8 Este; LCN = La Calandria Norte; LCS La Calandria Sur. (b) Geological map of the Loma Alta area. (c) Geological map of the La Calandria Sur area. Pink stars in (b) and (c) indicate sample collection locations. T, temperature; CBL, Bahía Laura Complex; Jr, Jurassic; K, Cretaceous; Tt, Tertiary; Qt, Quaternary. Figure modified from Guido and Campbell (2014). (For interpretation of the references to colour in this figure legend, the reader is referred to the web version of this article.)

characterised by a large Middle to Late Jurassic volcanic complex (Bahía Laura Complex), with several hydrothermal systems preserving epithermal mineral deposits in its later phases (Guido and Campbell, 2011). There are at least 23 hot spring related deposits exposed over a 230 × 230 km area (Guido and Campbell, 2011), including eight sinter deposits (Guido and Campbell, 2011). There are five major hot spring outcrop areas at the Claudia locality (Fig. 1; Guido and Campbell, 2014) – Loma Alta, La Calandria Sur, Lote 8, Lote 8 Este, and La Calandria Norte. The Loma Alta outcrop has been recognised as showing the best-preserved biogenic textures via petrographic analyses, followed by La Calandria Sur, where OM has been identified by Raman spectroscopy (Guido and Campbell, 2014; Guido et al., 2019).

The Loma Alta sinter outcrops (Fig. 1b) cover an area of 150 m × 50 m and are located at the intersection of two major faults, which may have served as conduits for the hydrothermal fluid discharge (Guido and Campbell, 2011). Outcrops include well-preserved vent geyserite that occurs in a sinter breccia, wavy laminated sinter, and sinter with plant material. In a Raman spectroscopy study from this site (Guido et al., 2019), abundant immature kerogen was found in samples from high-temperature geyseritic facies, mid-temperature sinter facies, and low-temperature sinter facies (Fig. 2).

The La Calandria Sur outcrops (Fig. 1c) cover a 1300 m × 400 m area and are hosted within a siliciclastic lacustrine sedimentary sequence (Guido and Campbell, 2014). An upper sinter comprises a clustering of several weathered geyseritic mounds of restricted areal extent, inferred as a hot spring vent complex, whereas the lower portion contains well-preserved plant-rich sinter (Guido and Campbell, 2014).

Overall, the Late Jurassic hydrothermal settings of the Deseado Massif serve as 'stepping stones' into the deep-time geological record, constituting intact palaeo-landscapes and palaeo-communities of spatially associated geothermal, lacustrine and fluvial environments in dynamic volcanic terrains (Guido et al., 2010; Guido and Campbell, 2011, 2014), comparable to the hydrothermal palaeoenvironments of nascent terrestrial landmasses on which early life on Earth took hold (Djokic et al., 2017, 2021; Van Kranendonk et al., 2021), and which potentially may have developed on Mars (Walter and Des Marais, 1993; Squyres et al., 2008; Skok et al., 2010; Ruff and Farmer, 2016; Ruff et al., 2020).

3. Materials and methods

3.1. Sampling

Sample 110a (Fig. 3a–c) was collected from the vent area associated with geyseritic sinter breccias at Loma Alta (Fig. 1b). Sample 121 (Fig. 3d–f) was collected from the lower sinter in the distal apron at La Calandria Sur (Fig. 1c). A basalt sample collected from the San Agustín palaeo-geothermal field, also located within the Deseado Massif, was used as a procedural blank. Samples were collected from each field site using gardening gloves, then wrapped in aluminium foil and were sent to the Macquarie University Organic Geochemistry laboratory. In the laboratory, samples were placed on ashed foil and broken with a sledgehammer, the head of which also was covered in ashed foil. Interior rock segments were plucked out with ashed foil and used in the molecular analyses. Remaining sinter portions were cut on a diamond saw at the University of New South Wales (UNSW) Sydney where they were photographed and then sent to Adelaide Petrography for thin section preparation.

3.2. Organic geochemistry preparation

Prior to all laboratory processes, all glassware, pipettes, aluminium foil and quartz sand were baked at 500 °C for 12 h to remove contaminants. Prior to baking the sand was extracted with dichloromethane (DCM) and methanol (MeOH) (9:1, v/v) by 3 × 10 min. sonication. Silica gel and glass wool for fractionation columns was also pre-extracted and combusted at 400 °C for 4 h. Powdering of the interior segments of the samples was conducted with a tungsten carbide ring mill. Before each sample was powdered, the ring and mill were cleaned by grinding and discarding extracted and baked sand at least three times, followed by washing with MeOH. Samples were submerged in DCM and MeOH (9:1, v/v) and extracted by sonication for 10 min, stirring, waiting five minutes, and sonication for another 10 min. After this the samples were stirred, and left to settle for five min, before being decanted into clean glassware. The process was repeated twice more for each sample. The second and third solvent mixtures were added to the first solvent mixture. Samples were evaporated by hotplate and a gentle stream of dried nitrogen. The samples were fractionated on small scale silica columns in Pasteur pipettes using a DCM:MeOH (4:1, v/v) mixture to elute the apolar fraction. The apolar fraction was further fractionated into aliphatic and aromatic hydrocarbons using hexane and the 4:1 solution, respectively. The fractions were spiked with 1 mL of an internal standard DCM solution containing about 117 ng each of anthracene-d_{10} (98 atom% D, Isotec), *p*-terphenyl-d_{14} (98 atom% D, Isotec), and tetracosane-d_{50} (98 atom% D, Isotec). The samples were reduced to 100 μL and pipetted into a vial insert before being analysed by gas chromatography–mass spectrometry (GC–MS).

3.3. Gas chromatography–mass spectrometry

3.3.1. Scan and single ion monitoring

Initial GC–MS analyses were carried out on an Agilent GC (6890N) coupled to an Agilent mass selective detector (5975B). A 1 mL portion of the aliphatic and aromatic fractions was injected into a programmable temperature vaporisation inlet operating in splitless mode (40 °C, 2 min hold, programmed to 310 °C (0.4 min, isothermal) at a rate of 700 °C/min, with a J&W DB5MS capillary column (60 m length, 0.25 mm i.d., 0.25 μm film thickness). Helium was used as the carrier gas (1.5 mL/min, constant flow), and the temperature of the GC oven was ramped from 40 °C (2 min isothermal) to 310 °C (40 min isothermal) at a rate of

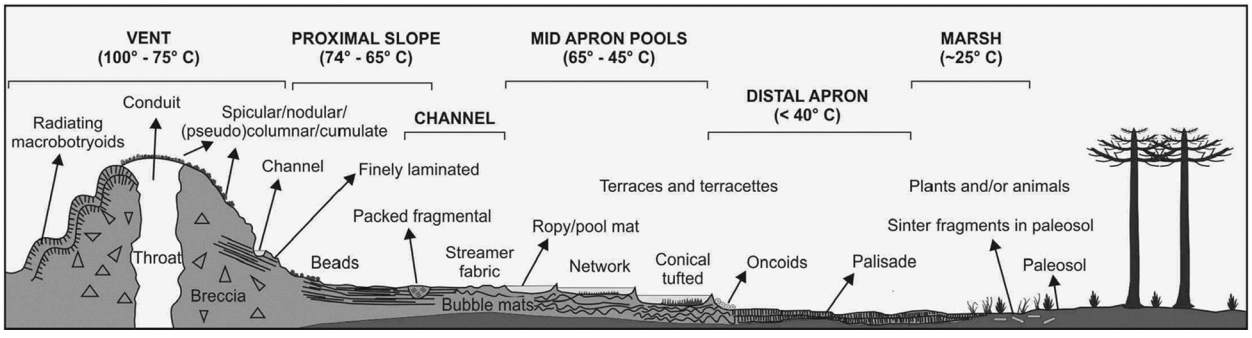

Fig. 2. Schematic cross-section of a near-neutral pH, alkali chloride, silica-bearing hot spring, illustrating vent to marsh facies. Sinter textures with environmental significance and temperature gradients are shown. Figure modified from Campbell et al. (2015).

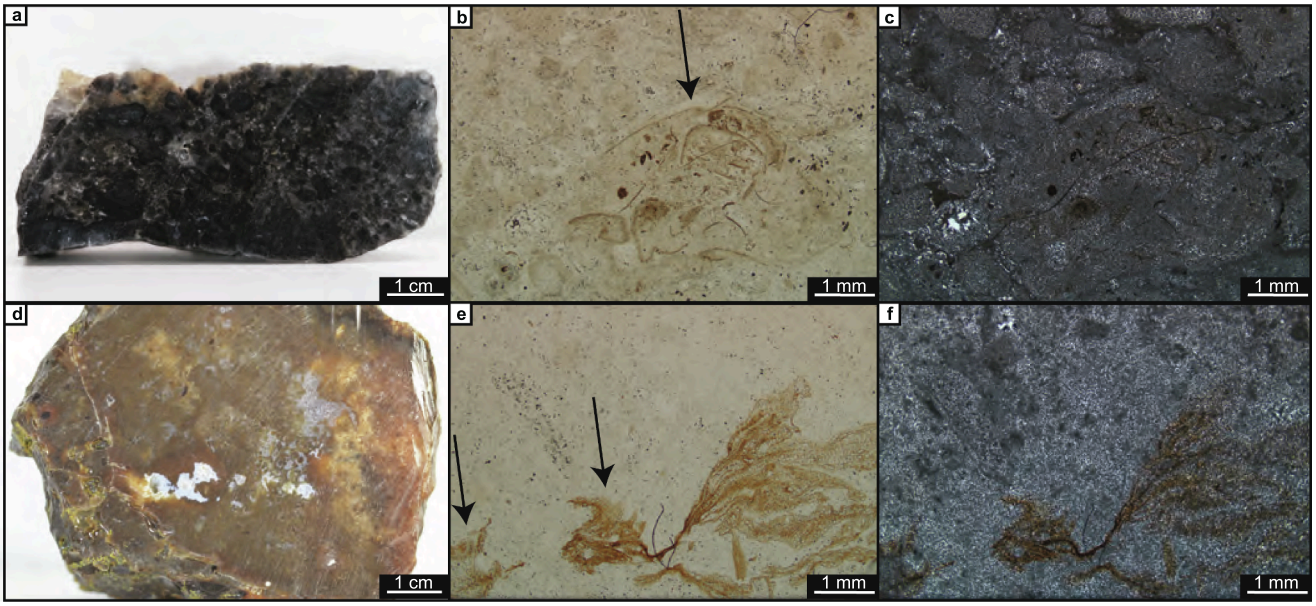

Fig. 3. Hand sample (a, d) and thin section images (b, c, e, f) of the studied samples. Sinter breccia sample 110a (a–c) and sample 121 (d–f) are shown. (a) Hand sample, (b) plane polarised light, (c) cross polarised light; (d) hand sample, (e) plane polarised light, (f) cross polarised light. Note the presence of light brown organic material in (b,c) and (e,f), indicated with arrows in (b) and (e).

4 °C/min. The mass spectrometry data were acquired in full scan (*m/z* 50–550) and single ion monitoring (SIM) modes (for a list of ions monitored please see Supplementary Table S1). Hydrocarbon identification was based on comparisons of relative GC retention times and mass spectra with a North Sea Oil standard. Semiquantitative analyses were performed on peak areas using the internal standard. The limit of detection was 5 pg/g.

3.3.2. *Metastable reaction monitoring*

Metastable reaction monitoring (MRM) analyses of cyclic biomarkers (steranes, diasteranes and hopanes) were performed using a Shimadzu GC–MS-TQ Nexis GC-2030. The samples were injected onto a J&W DB5MS capillary column (60 m lngth, 0.25 mm i.d., 0.25 μm film thickness) using a splitless injection technique with the inlet at 310 °C and the interface to the MS at 310 °C. The temperature of the GC oven was held at 40 °C for 2 min, ramped at 4 °C/min to 310 °C, and held for 45 min. The carrier gas was helium with a constant flow of 1.5 mL/min. The MS had an ion source temp of 250 °C and a detector voltage of 0.2 kV. MRM was achieved with argon collision gas, with a dwell time of 30 ms for each ion transition. A set of MS methods was developed to monitor parent/daughter ion transitions corresponding to different molecular weight steranes, diasteranes and hopanes (Supplementary Table S2). Peak areas for the calculation of biomarker ratios were determined separately using each ion transition.

4. Results

4.1. *Petrography*

Sinter breccia sample 110a from Loma Alta was collected from a sinter apron vent area (Figs. 1b and 2) with documented geyserite and related breccia (Supplementary Fig. S1a–c; Guido and Campbell, 2014). The sample is entirely silicified and comprises a matrix with microquartz mosaic texture and breccia clasts derived from different sources (Fig. 3b, c; Supplementary Fig. S1d–i). The breccia clasts are sub-rounded and composed of sinter, sinter breccia, volcaniclastic material, and fragments of euhedral/subhedral quartz crystals (Fig. 3; Supplementary Fig. S1). Some of the sinter clasts preserve remnants of plant fragments, along with fossilised microorganisms (Fig. 3b, c). Brecciation was likely phreatic, and the irregular rounded shapes of the clasts may be explained by clast attrition, followed by acidic fluids producing partial dissolution (i.e., holes in the sinter, Supplementary Fig. S1b, c, f, g). The breccia was then cemented by low temperature hot spring fluids to produce sinter rims of palisade microbial textures and matrix (now recrystallised) (Supplementary Fig. S1h, i). The sources of organic matter observed by petrography include fossil bacteria (Supplementary Fig. S1h, i) and plant fragments (Fig. 3b, c).

Fine-grained sinter sample 121 from La Calandria Sur is composed of rounded and sub-rounded clasts that contain abundant, low-temperature plant tissues (Fig. 3e, f; Supplementary Fig. S2a–d) typical of distal sinter aprons. The sample is fully silicified with a recrystallised matrix and voids filled with chalcedony and quartz (Supplementary Fig. S2e–f).

4.2. *Extractable hydrocarbons*

4.2.1. *n-Alkanes, isoprenoids, and carotanes*

The *n*-alkanes and isoprenoids of the studied samples were integrated in *m/z* 57 mass chromatograms acquired in SIM mode. Both samples contain *n*-alkane distributions with a convex shape (Fig. 4; Supplementary Fig. S3), with sample 110a ranging from $C_{17–38}$, and sample 121 ranging from $C_{14–33}$. *n*-Alkanes are more abundant in sample 121 than sample 110a, but both samples have a slight odd-over-even carbon number predominance for the *n*-alkanes, indicated by a carbon preference index ($CPI_{22–32}$) of 1.14–1.23. Pristane (Pr) and phytane (Ph) were also detected in both samples, with a Pr/Ph ratio of 1.2 (Table 1). γ-Carotane and β-carotane are present in sample 121, together with some tentatively identified carotenes (Fig. 4b).

4.2.2. *Methylalkanes*

Monomethylalkanes (MMAs) were detected in both samples, from $C_{18–33}$ in sample 110a and from $C_{16–31}$ in sample 121 (Fig. 4). Both samples contain methylheptadecanes (MHeD) in which the mid-chain MHeDs are more predominant than 2-MHeD and 3-MHeD (Fig. 4). In contrast, the distribution of MMAs varies between the samples. In sample 110a, the 2- and 3-methyl isomers are the most dominant, except at $C_{18,19,23,25,26,27}$ where the mid-chain MMAs are more prominent. In sample 121, the mid-chain MMAs are of equal abundance to the 2- and

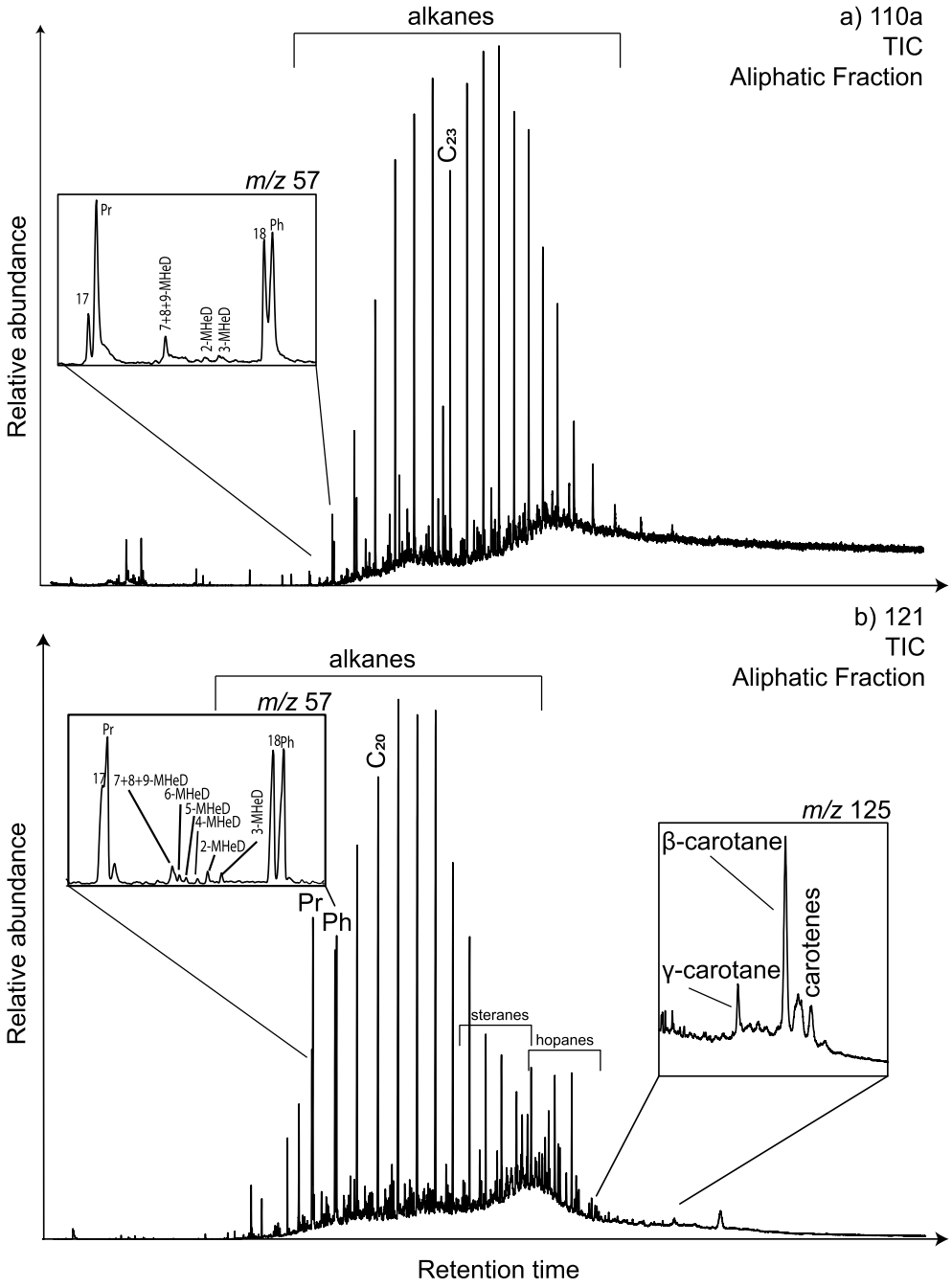

Fig. 4. Total ion chromatograms of the aliphatic fraction of; (a) sample 110a, and (b) sample 121. Insets in (a) and (b) are from single ion monitoring runs (partial *m/z* 57 and 125 mass chromatograms). Pr = pristane; Ph = phytane; MHeD = methylheptadecane; numbered peaks refer to *n*-alkanes.

3-methyl isomers from C_{16}–C_{23}, (except in the case of the MeDs), but at higher molecular weights the 2- and 3-methyl isomers become the dominant ones.

4.2.3. Cyclic biomarkers

Cyclic biomarkers detected include hopanes, steranes, and diasteranes, which were integrated in MRM chromatograms.

4.2.3.1. Hopanes and methylhopanes. Both samples contain C_{27} to C_{35} hopanes (pentacyclic triterpanes; Fig. 5). The C_{27} hopanes in both samples are dominated by 17α(H)–22,29,30-trisnorhopane (Tm) with appreciable amounts of 17β(H)–22,29,30-trisnorhopane (B), and lesser amounts of 18α(H)–22,29,30-trisnorneohopane (Ts). The Ts/(Ts + Tm) ratio is 0.30 for sample 110a and 0.15 for sample 121, and the Tm/(Tm + B) ratio is 0.63 and 0.70, respectively (Table 1). Dinorhopanes (DNH) are present in both samples, with 28,30-DNH > 25,30-DNH > 29,30-DNH, but they are in low abundance relative to the other hopanes (Fig. 5). The dominant hopanes in both samples are the $C_{29–31}$ αβ isomers, with smaller amounts of moretanes (βα). ββ hopanes from $C_{29–32}$ are present in very low amounts (<1% of C_{30} αβ hopane) in sample 121, but were not detected in sample 110a. The abundance distribution of the hopanes in the *m/z* 191 mass fragmentogram is $C_{30} > C_{29} > C_{27} > C_{31}$. Homohopanes from C_{31}–C_{35} are present with both 22S and 22R epimers, decreasing in abundance from C_{31} to C_{35} (Fig. 5). In sample 110a the C_{31} and C_{33} αβ 22S/(22S + 22R) ratios are 0.46, showing a 22R predominance, but the C_{32} 22S/(22S + 22R) ratio is at equilibrium (0.62; Table 1). The C_{31}–C_{33} homohopane ratios for sample 121 vary from 0.36 to 0.42.

Table 1
Hydrocarbon ratios for the samples from the Claudia hot springs.

Ratio	Sample 110a	Sample 121
Pristane/phytane	1.2	1.2
Pristane/*n*-C_{17}	4.4	1.6
Phytane/*n*-C_{18}	1.2	0.87
Carbon preference index of *n*-alkanes ($CPI_{22\text{-}32}$)	1.1	1.2
Ts/(Ts + Tm)	0.30	0.15
Tm/(Tm + B)	0.63	0.70
C_{29} αβ hopane/C_{30} αβ hopane	0.51	0.35
C_{29} αβ/(αβ + βα) hopanes	0.76	0.70
C_{30} αβ/(αβ + βα) hopanes	0.92	0.91
C_{31} αβ 22S/(22S + 22R) hopanes	0.46	0.42
C_{32} αβ 22S/(22S + 22R) hopanes	0.62	0.36
C_{33} αβ 22S/(22S + 22R) hopanes	0.46	0.38
C_{31} αβ hopane/C_{30} αβ hopane	0.26	0.20
C_{29}Ts/(C_{29}Ts + C_{29} αβ hopane)	0.25	0.12
C_{35}/(C_{35} + C_{34}) homohopanes	0.48	0.28
28,30-bisnorhopane/C_{30} αβ hopane	0.05	0.05
Gammacerane/C_{30} αβ hopane	0.18	0.14
C_{27} αββ/(αββ + ααα) steranes	0.11	0.09
C_{29} ααα 20S/(20S + 20R) steranes	0.20	0.14
C_{27} βα 20S/(20S + 20R) diasteranes	0.50	0.49
C_{27} βα diasteranes/(ααα + αββ) steranes	1.05	1.18
C_{29}/C_{27} ααα 20R steranes	3.6	5.0
C_{28}/C_{29} ααα 20R steranes	0.30	0.26
(24/(24 + 27) nordiacholestanes (NDR)	nd	0.46
(24/(24 + 27) norcholestanes (NCR)	nd	0.62
Triaromatic steroid index	0.2	0.2
Methylnaphthalene ratio (MNR; 2-MN/1-MN)	1.1	1.2
Dimethylnaphthalene ratio-1 (DNR-1)	4.1	3.3
Trimethylnaphthalene ratio-1 (TNR-1)	1.17	1.05
Trimethylnaphthalene ratio-2 (TNR-2)	0.40	0.69
Trimethylnaphthalene ratio (TMNr)	0.38	0.11
Tetramethylnaphthalene ratio (TeMNr)	nd	0.54
Methylphenanthrene index (MPI)	0.53	0.83
Methylphenanthrene distribution fraction (MPDF)	0.34	0.47
Phenanthrene/anthracene	8.8	9.7
2-Methylphenanthrene/2-methylanthracene	0.61	6.2
Dimethylphenanthrene ratio (DMPR-x)	0.39	0.51
Retene/9-methylphenanthrene	2.2	12.7
Fluoranthene/(fluoranthene + pyrene)	0.28	0.37
3-Methylbiphenyl/2-methylbiphenyl	0.96	2.2
Phenanthrene/dibenzothiophene	13.7	13.7

Carbon preference index of *n*-alkanes: $(2 \times (C_{23} + C_{25} + C_{27} + C_{29} + C_{31}))/(C_{22} + 2 \times C_{24} + 2 \times C_{26} + 2 \times C_{28} + 2 \times C_{30} + C_{32})$; Triaromatic steroid index = (TA (I)/(TA(I + II)); DNR-1 = ([2,6-DMN + 2,7-DMN])/1,5-DMN); TNR-1 = (2,3,6-TMN/[1,4,6- + 1,3,5-TMN]); TNR-2 = ([2,3,6- + 1,3,7-TMN]/[1,4,6- + 1,3,5- + 1,3,6-TMN]); TMNr = 1,3,7-TMN/(1,3,-TMN + 1,2,5-TMN); TeMNr = 1,3,6,7-TeMN/(1,3,6,7-TeMN + 1,2,5,6-TeMN); MPI = methylphenanthrene index (1.5 × (3-MP + 2-MP)/(P + 9-MP + 1MP)); MPDF = (3-MP + 2-MP)/total MPs); DMPR = 1,7-DMP/(1,7-DMP + 1,3-DMP + 3,9-DMP + 2,10-DMP + 3,10-DMP); nd = not determined. All biomarker ratios were determined from MRM transitions.

Gammacerane is present in small amounts in both samples. A putative 2-methylgammacerance was detected in MRM (Supplementary Fig. S4) and was tentatively confirmed in full scan mode based on retention time and coelution with 3β-methylhopane (Grosjean et al., 2012), and spectral identification (Supplementary Fig. S5). The spectrum had the characteristic main fragment ion of *m/z* 205 instead of *m/z* 191, and a molecular ion at *m/z* 426 (compare with Duda et al., 2020).

Sample 110a contains C_{32} 3β-methylhopanes (both αβ and βα 22S + 22R). Sample 121 contains $C_{31\text{-}34}$ 2α- and 2β-methylhopanes, and $C_{31\text{–}32}$ 3α- and 3β-methylhopanes (Supplementary Fig. S4). For the $C_{31\text{-}32}$ isomers, 2α-methylhopane is more abundant than 2β-methylhopane, whereas for C_{33} the 2β-methylhopane is larger than the 2α-methylhopane.

4.2.3.2. Steranes, diasteranes and branched steranes. Sample 110a contains $C_{27\text{-}29}$ steranes and diasteranes, with a relative abundance of $C_{29} > C_{27} > C_{28}$ (Fig. 6; Table 1). Sample 121 contains $C_{26\text{-}30}$ steranes and diasteranes, with a relative abundance of $C_{29} > C_{27} > C_{28} > C_{30} > C_{26}$. Sample 121 contains 3-ethylcholestanes, 24-methylcholestanes, 3-propylcholestanes, and 24-ethylcholestanes, but no dinosteranes were detected in the *m/z* 414 → 98 MRM transition. Sample 121 contains readily detectable C_{26} norcholestanes and nordiacholestanes, with a norcholestane ratio (NCR) of 0.62, and a nordiacholestane ratio (NDR) of 0.46, but these molecules were not detected in sample 110a (Fig. 6). Diasteranes are generally of similar abundance as the regular steranes in both samples (Fig. 6). Both samples also have low C_{27} αββ/(αββ + ααα) ratios (0.09, 0.11; Table 1). The C_{29} ααα 20S isomer is less abundant than the C_{29} ααα 20R isomer, with C_{29} ααα sterane 20S/(20S + 20R) ratios of 0.14 (sample 121) and 0.20 (samples 110a). In both samples it is inferred that the C_{28} and C_{29} βαα isomers are present, coeluting with the αββ 20R isomers, as evident by the much higher apparent abundance of the αββ 20R isomers compared to the αββ 20S isomers (Fig. 6). There is no compelling evidence from the 372 → 217 MRM transition for the C_{27} βαα isomer in either sample, although it might be present.

The peaks present in the 414 → 217 MRM transition of sample 121 are mainly methylsteranes rather than *n*-propylcholestanes. Branched steranes were detected in sample 121 (Supplementary Fig. S6) but not in sample 110a. 3-Ethylcholestanes, 24-methylcholestanes, 3-propylcholestanes are present, and the methyl-24-ethylcholestanes in the *m/z* 414 → 231 chromatogram include 2α-, 2β-, 3β- and 4α-methylsteranes (Supplementary Fig. S6).

4.2.4. Aromatic compounds

All aromatic compounds were integrated from SIM data. Both studied samples contain naphthalene, phenanthrene, anthracene, retene, dibenzothiophene (DBT), biphenyl, fluorene, fluoranthene (Fl), pyrene (Py), chrysene (Ch), triphenylene (Trip), benzo[*a*]anthracene (BaA), and coronene (Co), as well as some of their alkyl derivatives. The alkylnaphthalenes (Fig. 7) include dimethylnaphthalenes (DMN), trimethylnaphthalenes (TMN), tetramethylnaphthalenes (TeMN) and pentamethylnaphthalenes (PMN). The relative abundance of alkylnaphthalenes in sample 110a is dominated by DMN (~70% of total alkylnaphthalenes), but TMN and TeMN predominate in sample 121 (TEMN + TMN > 95% of total alkylnaphthalenes) (Fig. 7). In both samples 2-MN is slightly more abundant than 1-MN, but in sample 110a the MNs are 10× larger relative to naphthalene. The abundance of ethylnaphthalenes (EN) is low compared to DMNs in both samples (total EN is < 3% of total EN + DMN). The most abundant TMN isomer in sample 110a is 1,3,6-TMN, while 1,2,5-TMN is the most abundant isomer in samples 121. In sample 121, 1,3,6,7-TeMN and the coeluting 1,2,5,6- and 1,2,3,5-TeMN are the most abundant TeMN compounds. The methylnaphthalene ratios of the samples are 1.1 and 1.2. The dimethylnaphthalene ratio, trimethylnaphthalene ratio (TMNr) and trimethylnaphthalene ratio-1 are lower for sample 121, but the trimethylnaphthalene ratio-2 is higher for sample 121 (Table 1). The tetramethylnaphthalene ratio could not be calculated for sample 110a due to the absence of any TeMNs (Fig. 7), and is 0.54 for sample 121.

The alkylphenanthrenes are composed of methylphenanthrenes (MP), ethylphenanthrenes and dimethylphenanthrenes (DMP). 9-MP is the dominant MP isomer in sample 110a, while 2-MP is more abundant than 9-MP in sample 121. Anthracene, 2-methylanthracene (MA) and 1-MA are present in both samples. Phenanthrene is more than 8× the abundance of anthracene in both samples, and the phenanthrene/anthracene ratio is slightly lower in sample 110a. Sample 110a contains a significantly larger amount of 2-MA than sample 121 (Table 1). The most abundant peak due to DMPs in sample 110a is the peak due to coeluting 1,3- + 3,9- + 2,10- + 3,10-DMP, which is also a significant peak in sample 121. However, 1,7-DMP is more abundant relative to other DMPs in sample 121 than in sample 110a (Fig. 7; Table 1). Retene is present in significant amounts in both samples, although is a much larger component in sample 121 (retene/9-MP = 12.7) than in sample 110a (retene/9-MP = 2.2) (Table 1). The methylphenanthrene

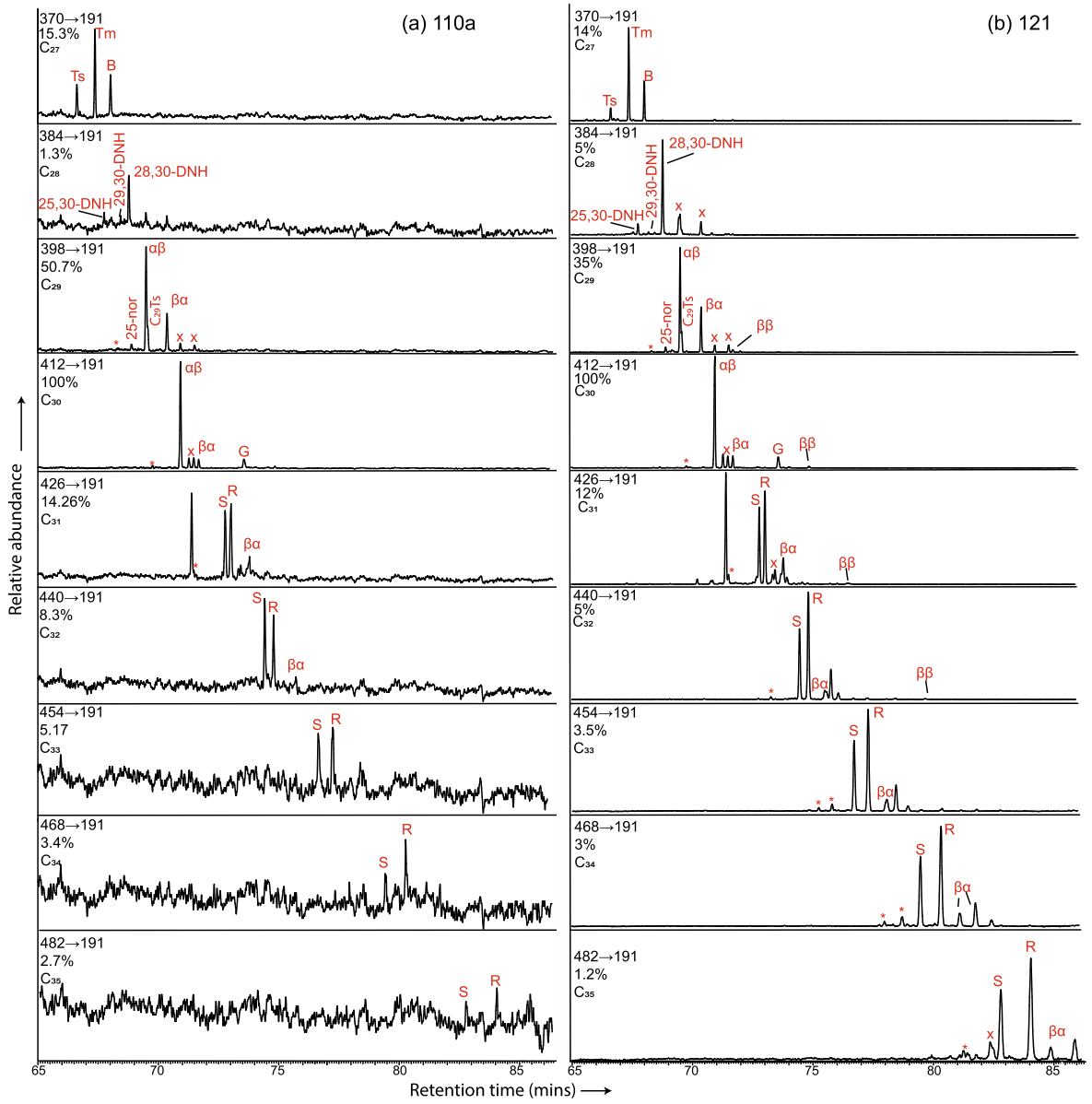

Fig. 5. Metastable reaction monitoring (MRM) chromatograms showing the hopane distributions in samples (a) 110a and (b) 121. Peak assignments define the stereochemistry at C-22 (S and R); αβ, βα and ββ denote 17α(H),21β(H), 17β(H),21α(H) and 17β(H),21β(H), respectively; Ts = 18α(H)–22,29,30-trisnorneohopane; Tm = 17α(H)–22,29,30-trisnorhopane; B = 17β(H)–22,29,30-trisnorhopane; DNH = dinorhopane; nor = norhopane; G = gammacerane; * = diahopane; x = cross talk or unknown. Numbers are % height of MRM chromatograms.

distribution fraction and the methylphenanthrene index are both higher for sample 121 (Table 1).

Both samples contain biphenyl and methylbiphenyls (Fig. 7), and the 3-methylbiphenyl/2-methylbiphenyl ratio is higher in sample 121 (Table 1). Sample 121 contains both fluorene and dibenzothiophene (fluorene > DBT), but sample 110a contains only dibenzothiophene. In both samples phenanthrene is more abundant than dibenzothiophene (P/DBT = 13.7). Methylfluorenes are present with 1-MF the most abundant isomer, but methyldibenzofurans, methyldibenzothiophenes and dimethyldibenzothiophenes are not present in the samples.

$C_{20\text{-}21}$ and $C_{26\text{-}28}$ triaromatic steroids are present in both samples (Supplementary Fig. S7). The triaromatic steroid index (TA(I)/TA(I + II)) (Mackenzie et al., 1981) for both samples is 0.02.

The 4-ring aromatic hydrocarbons fluoranthene, pyrene, chrysene, triphenylene and benzo[*a*]anthracene are the most predominant aromatic compounds in sample 110a (Py > Fl > Trip > Ch > BaA). These polycyclic aromatic hydrocarbons are also present in sample 121, but are of similar abundance to the rest of the compounds (Py > Fl > Ch > Trip > BaA). In both samples Fl/(Fl + Py) is < 0.4. Coronene is present in large abundance in sample 110a (Co > Ch), and is present in low abundance in sample 121 (BaA > Co).

4.2.5. *Contamination control*

Basalt collected from the San Agustín sinter locality in the Deseado Massif was analysed as a cumulative laboratory blank (Supplementary Fig. S3b). Some *n*-alkanes were detected in SIM mode but not in scan mode for this sample, whereas no aromatic compounds or cyclic biomarkers were detected. The series of $C_{19\text{–}40}$ *n*-alkanes detected in the blank have a strong odd-over-even predominance, a maximum at C_{27} (0.5 ng/g), and a different distribution than the samples discussed here (Supplementary Fig. S3b). When these *n*-alkanes are subtracted from the *n*-alkanes detected in the samples, some very slight differences in the distribution above C_{32} are notable in sample 110a, but the differences are not evident in sample 121 (Supplementary Fig. S3b).

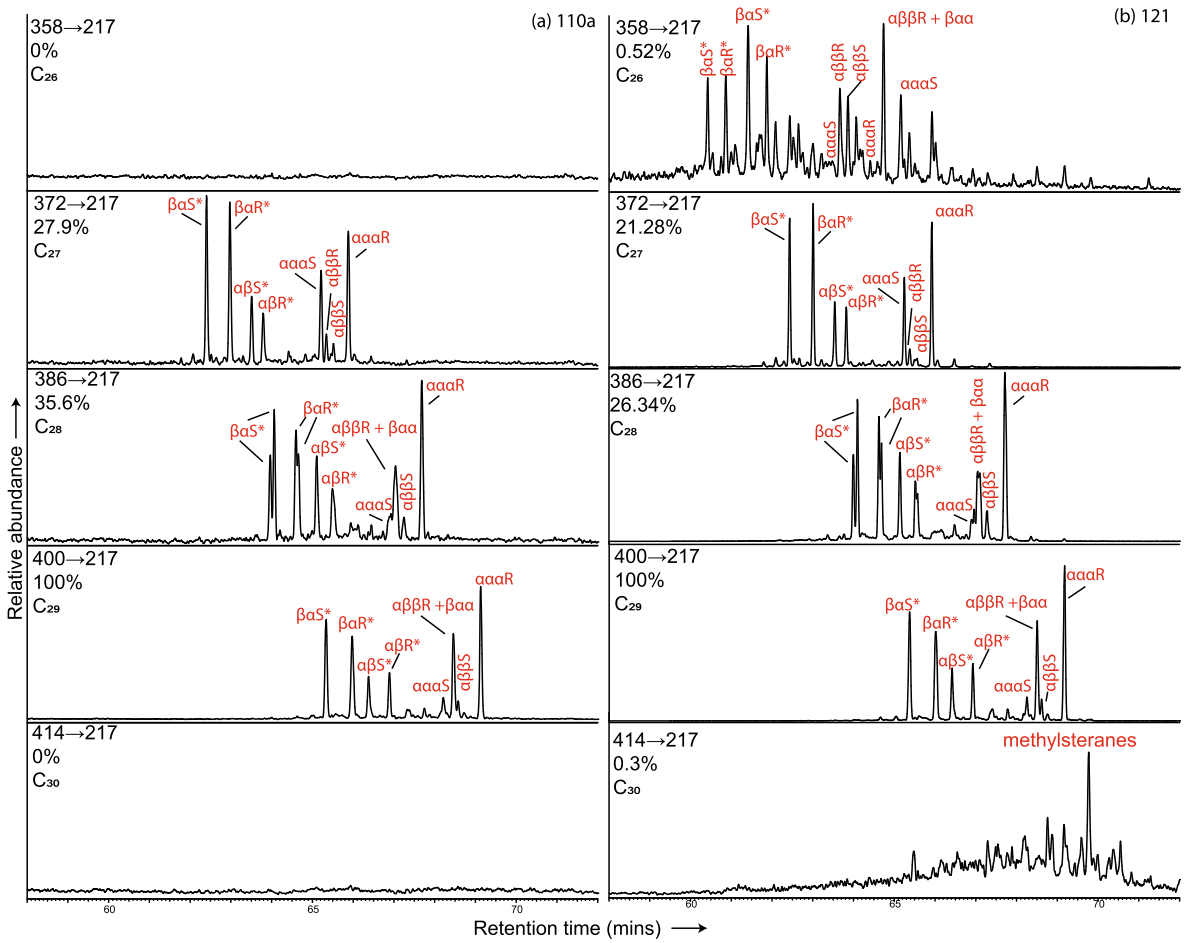

Fig. 6. Metastable reaction monitoring chromatograms of steranes and diasteranes present in samples (a) 110a and (b) 121. Peak assignments define the stereochemistry at C-20 (S and R). βα, αβ, ααα, αββ and βαα denote 13β(H),17α(H)-diasteranes, 13α(H),17β(H)-diasteranes, 5α(H),14α(H),17α(H)-steranes, 5α(H),14β(H),17β(H)-steranes, and 5β(H),14α(H),17α(H)-steranes, respectively. * = diasterane. Numbers are % height of MRM chromatograms.

No phthalates or branched alkanes with a quaternary carbon were detected in samples 110a and 121. Some siloxanes were detected in the column bleed of some GC runs of these samples, but these do not co-elute with any of the target compounds analysed.

5. Discussion

5.1. Sources of organic matter

The dominant OM signal within these samples is derived from terrigenous sources. The Pr/*n*-C_{17} ratios of 1.6 and 4.4 of the studied samples are high and consistent with a low thermal maturity, and they are also a signature of oxidised terrigenous OM (Hakimi et al., 2018). The slight odd-over-even carbon number predominance for the high molecular weight *n*-alkanes (Table 1), especially in the C_{27}, C_{29}, and C_{31} *n*-alkanes, is commonly associated with the waxes of vascular plants (Eglinton and Hamilton, 1967), a conclusion consistent with the petrographic observations of higher plant fossils in both samples (Fig. 3; Supplementary Fig. S2).

Aromatic hydrocarbons such as naphthalene, anthracene, retene and chrysene are typically indicative of terrigenous higher plant input (Chaffee and Johns, 1983; Chaffee et al., 1984). 1,7-DMP is reported to be associated with higher plants (e.g., pimaric acid) (Alexander, 1992; Alexander et al., 1992), and is more abundant in sample 121 than sample 110a (Table 1; Fig. 6). Similarly, retene is associated with the resins containing abietic acid derived from coniferous plants (e.g., van Aarssen et al., 2000), although other sources are possible (e.g., Romero-Sarmiento et al., 2010); this compound is also much more abundant in sample 121 than sample 110a (Table 1; Fig. 6). A major component of the OM from terrigenous sources is also supported by the high proportion of C_{29} steranes relative to other steranes (Moldowan et al., 1985).

In addition, a bacterial source of OM in the studied samples is supported by the presence of hopanes, MMAs (in particular MHeDs), 28,30-DNH, and petrography (Supplementary Fig. S1h, i). Hopanes are saturated molecules preserved in sedimentary rocks that are derived from hopanoids in bacterial membranes (Ourisson et al., 1979). MHeDs can be derived from cyanobacteria, which are the only microorganisms known to directly produce these hydrocarbons (Fig. 4; Schirmer et al., 2010), although MHeDs and MMAs more generally are present in many rocks and oils in thermodynamic isomeric equilibrium due to thermal maturation processes (e.g., Kissin, 1993). 2α- and 2β-methylhopanes detected in sample 121 are compounds that Summons et al. (1999) suggested are biomarkers for cyanobacteria based on the appearance of their biological precursors (2α-methylbacteriohopanepolyol) in cultured cyanobacteria and cyanobacterial mats. However, it has subsequently been determined that 2α-methylhopanes occur in other bacterial strains as well, including alpha-proteobacteria and anoxygenic phototrophs (Rashby et al., 2007; Welander et al., 2010; Eickhoff et al., 2013). The presence of significant amounts of 2β-methylhopanes in sample 121 is consistent with excellent geochemical preservation of the biomarkers, as they are less stable than the 2α-methylhopanes (Summons and Jahnke, 1992).

A specific cyanobacterial origin is shown by a predominance of the mid-chain MMA isomers (Shiea et al., 1990, 1991; Kenig et al., 1995;

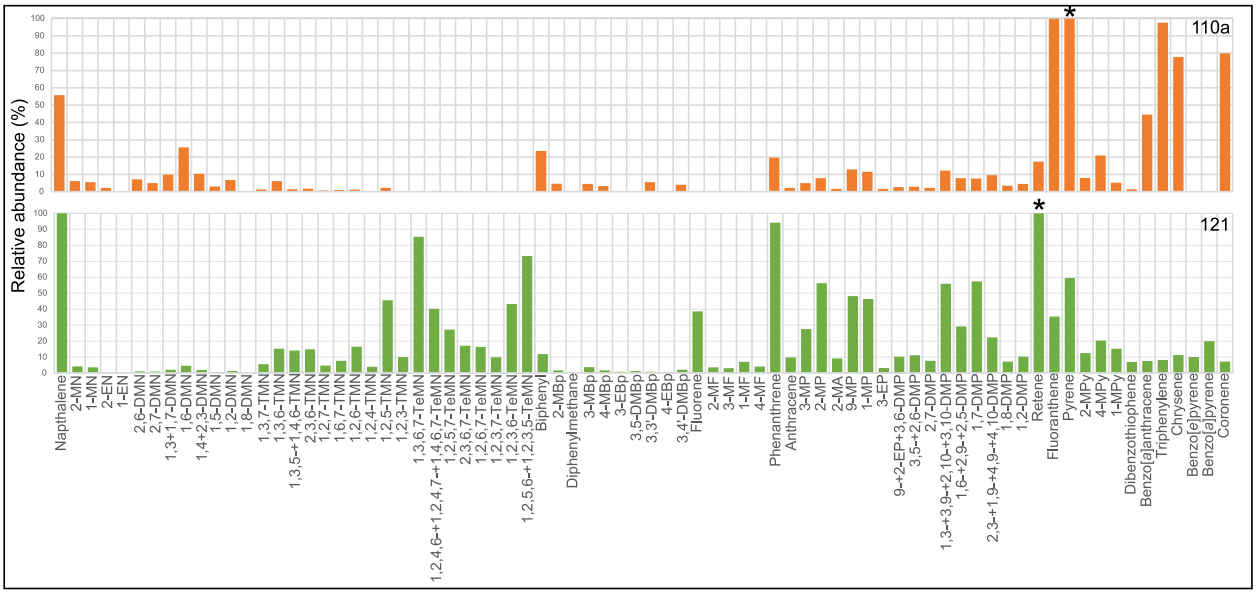

Fig. 7. Relative abundance of aromatic compounds in samples 110a (orange; relative to fluoranthene) and 121 (green; relative to naphthalene). Compounds with an asterisk exceed the maximum abundance shown: in sample 110a pyrene was 259% of fluoranthene; in sample 121 retene was 412% of naphthalene. MN = methylnaphthalene; EN = ethylnaphthalene; DMN = dimethylnaphthalene; TMN = trimethylnaphthalene; TeMN = tetramethylnaphthalene; MBp = methylbiphenyl; EBp = ethylbiphenyl; DMBp = dimethylbiphenyl; MF = methylfluorene; MP = methylphenanthrene; MA = methylanthracene; EP = ethylphenanthrene; DMP = dimethylphenanthrene; MPy = methylpyrene. (For interpretation of the references to colour in this figure legend, the reader is referred to the web version of this article.)

Schirmer et al., 2010; Hoshino and George, 2015). For example, a predominance of 7- and 8-MHeDs over terminal isomers is common in hot spring cyanobacterial mats (Robinson and Eglinton, 1990; Shiea et al., 1990; Teece et al., 2020). The presence of 2- and 3-substituted MMAs can be linked to either inorganic processes or to bacteria, as some sulfate-reducing bacteria have been known to produce the biological precursors to 2- and 3-MMAs (Peckmann et al., 2004). The presence of 28,30-DNH is indicative of a source from chemoautotrophic bacteria (Schoell et al., 1992). Methanotrophic and acetic acid bacteria produce 3β-methyl bacteriohopanepolyols (Rohmer et al., 1984; Zundel and Rohmer, 1985), which are the unsaturated precursors to the 3β-methylhopanes, the latter of which are compounds detected in this study. Furthermore, the presence of 3-ethylcholestanes in sample 121 is evidence of bacterial reworking during diagenesis (Summons and Capon, 1991).

An algal source for some of the OM in the samples is supported by the presence of the C_{27} and C_{28} steranes (Volkman et al., 1987), as well as the presence of 4α-methyl-24-ethylcholestanes (Supplementary Fig. S5; Summons et al., 1987; Aboglila et al., 2011). Dinosterol and related sterols are the precursors of dinosteranes and triaromatic dinosteroids, and are produced by dinoflagellates (Withers, 1983; Volkman et al., 1990).

The presence of γ-carotane and β-carotane in sample 121 (Fig. 4b) is suggestive of an anoxic, saline, lacustrine or restricted marine setting where algae (such as *Dunaliella*) may be abundant (Jiang and Fowler, 1986). The NDR and NCR (Table 1) are commonly used to assess the source and age of OM. 24-Norcholestanes are thought to be derived from diatom blooms (e.g., Volkman et al., 1987), and therefore these ratios can be used as an age tracer related to the evolution and proliferation of diatoms (Holba et al., 1998). Typical Jurassic values of NCR are 0.02–0.26, whereas sample 121 has a value of 0.62, more consistent with the Cenozoic. However, these calibrant NCRs are derived from petroleum source rocks, not hot springs. While we do not observe diatoms within the Claudia samples, hot spring silica is diatomaceous in the distal sinter (e.g., Fernandez-Turiel et al., 2005; Owen et al., 2008). Diatom silica has poor preservation potential, and the textural signal of diatoms is blurred by dissolution and recrystallisation, so fossil diatoms are less likely to be preserved in geothermal deposits older than the Neogene (Jones and Renaut, 2007; Owen et al., 2008). Therefore, the high NCR and NDR values in sample 121 are consistent with the hot spring environment from which the OM has been derived.

Large multi-ring aromatic hydrocarbons are sometimes associated with heat sources. Several 4- to 7-ring aromatic compounds are more dominant in sample 110a than sample 121 (Fig. 7); these include pyrene, benzo[*a*]pyrene, benzo[*e*]pyrene (in sample 121 only), and fluoranthene, compounds previously linked to combustion-related sources (i.e., wildfires) (Huang et al., 2015). The large relative amount of coronene in sample 110a (Fig. 7) may also be related to a pyrolytic origin in palaeo-wildfires (Zakrzewski et al., 2020; Zakrzewski and Kosakowski, 2021). The Fl/(Fl + Py) ratios can discriminate between petrogenic and combustion inputs (<0.4 for petrogenic and >0.5 for combustion) (Yunker et al., 2002). However, the Fl/(Fl + Py) ratios for these samples (0.28, 0.37) fall into the petrogenic range, again suggesting multiple sources for the OM.

5.2. Depositional environments

The two samples studied here come from different parts of the Claudia sinter facies temperature gradient (cf. Fig. 2). Sample 110a constitutes a hydrothermal eruption breccia from the proximal sinter apron area. This type of breccia forms when solid material is forcibly ejected through hydrothermal vents by steam eruptions from the subsurface. The fragments within such breccias are poorly sorted and can have varied sources, including those from deep within geothermal reservoirs as well as surface materials (Browne and Lawless, 2001).

Hydrothermal breccias typically form at >100 °C, as geothermal fluids in the subsurface undergo a change in pressure to cause a steam-heated eruption (Browne and Lawless, 2001; Montanaro et al., 2020; Kilgour et al., 2021). While breccias can be generated in any part of a hydrothermal system, when they contain sinter clasts (Fig. 3; Supplementary Fig. S1) and are associated with geyserite (e.g., the site of sample 110; Guido and Campbell, 2014), they are spatially constrained to have been deposited at the surface in the near-vent area (Hamilton et al., 2019). In fact, hydrothermal brecciation may facilitate fluid up-

flow from deeper chloride-rich geothermal reservoirs to initiate the formation of surface hot-springs, such as those that created Champagne Pool ~ 700 years B.P. at the Wai-O-Tapu geothermal area in New Zealand (Gallagher et al., 2020). Such a scenario was likely for the Claudia vent area at the site of sample 110, since sinter and other breccia clasts derived from the hydrothermal eruption were subsequently coated in palisade microbial sinter (Supplementary Fig. S1h, i).

In contrast, sample 121 was collected from a geothermally influenced marsh area in the distal apron. These depositional environments occur at <40 °C, where the biota silicifies as it is bathed in the tepid to cool geothermal fluids debouching into low marshy areas (Trewin et al., 2003; Hamilton et al., 2019).

The Pr/Ph ratios of 1.2 for the samples (Table 1) is weakly correlated with depositional environments, suggesting suboxic conditions (Powell and McKirdy, 1973; Didyk et al., 1978). These values are inconsistent with Pr/Ph ratios reported from other hot springs, which are typically below 1 due to hypersaline conditions (Reinhardt et al., 2019; Teece et al., 2020). These results likely represent a mixture of signal from the hot spring system itself and the surrounding marsh area. Gammacerane, a biomarker tracer for tetrahymanol, was detected in both samples, which further supports the chloride thermal fluid conditions expected, as gammacerane is thought to represent a saline environment or, more generally, deposition within a stratified water column in palaeoenvironments (Chen and Summons, 2001), again showing that the OM contains a mixture of signals from different depositional conditions.

Summons and Jahnke (1990) observed that 2α-methylhopanes are typically more abundant than 3β-methylhopanes in ancient sediments and petroleum, and are often abundant in hypersaline depositional environments. Both of these compound groups are found in sample 121 (Supplementary Fig. S4), and C_{32} 3β-methylhopanes were detected in sample 110a, consistent with a microbially varied and possibly hypersaline depositional environment. However, the gammacerane/C_{30} αβ hopane ratio is relatively low in both samples (<0.2; Table 1), consistent with the Pr/Ph ratios that indicate hypersalinity was not a dominant depositional feature in these hot springs.

The presence of large relative amounts of diasteranes in the samples (Table 1) is likely not a result of abundant clay minerals relative to total organic carbon content, with which they are commonly associated (van Kaam-Peters et al., 1998). This is because there is no evidence of clays in the petrographic or other studies from this hot spring locality. Instead, we propose the clays may have been associated with the oxic terrigenous OM in the distal marsh area, which also explains why no diahopanes are present. Alternatively, oxic and acidic conditions can facilitate diasterane formation during diagenesis. There is evidence for oxic OM in the Pr/*n*-C_{17} ratios (Hakimi et al., 2018). Additionally, there is petrographic evidence of acid overprinting and dissolution (Fig. 3b, c; Supplementary Fig. S1f, g).

The phenanthrene/anthracene and 2-MP/2-MA ratios (Table 1) can be used as source parameters, and are often higher in coals, coal tars, and igneous intrusion-related oils or sediments (Radke et al., 1982b; Kissin, 1993; Li et al., 1998; Huang et al., 2015). The higher amounts of anthracene and 2-MA in sample 110a is consistent with a significant contribution of pyrolyzed terrigenous OM. The presence of 28,30-DNH and β-carotane in sample 121 indicates that while some of the OM was derived from an oxic, terrigenous environment, other portions of the OM were derived from an anoxic environment (Jiang and Fowler, 1986; Schoell et al., 1992), consistent with wet, marshy conditions inferred for the site.

5.3. Thermal maturity of organic matter

The majority of the biomarker thermal maturity ratios indicate that both of the Jurassic samples investigated here are thermally immature, with sample 121 being the least mature. However, there is an indication from some hopane ratios (C_{30} αβ/(αβ + βα); C_{32} 22S/(22S + 22R)) of some maturity discrepancies, which could relate to a source influence or some mixing of a high maturity component.

The Ts/(Ts + Tm) ratios for the samples (0.3, 0.15) indicate that the Claudia samples are immature (vitrinite reflectance equivalent (VRE) < 0.6%; Table 2) (Seifert and Moldowan, 1978). The Ts/(Ts + Tm) and C_{29}Ts/(C_{29}Ts + C_{29} αβ hopane) ratios are lower for sample 121 (distal apron) than sample 110a (vent breccia). There are large amounts of 17β(H)–22,29,30-trisnorhopane in both samples, giving clear evidence of low thermal maturity. The C_{29} αβ/(αβ + βα) hopane ratios (0.70, 0.76) for samples 121 and 110a, respectively, are below thermal equilibrium and consistent with this relative thermal maturity difference (Killops and Killops, 2013). However, the C_{30} αβ/(αβ + βα) hopane ratios at Claudia are at, or close to, equilibrium of ~0.92. The C_{31}–C_{33} αβ 22S/(22S + 22R) ratios for the samples at Claudia – except for the thermally mature C_{32} homohopane from sample 110a – are much lower than those reported in the Pleistocene (0.49–0.61; Reinhardt et al., 2019) which have surpassed VRE = 0.55% (Table 2) (Killops and Killops, 2013). These homohopane ratios mostly indicate that the samples in this study have a VRE < 0.55% (Table 2), and thus are very well preserved (Seifert and Moldowan, 1980). The presence of traces of unstable ββ hopanes in the distal apron (sample 121) (Fig. 5) further illustrates its thermal immaturity compared to the vent sample (110a) (Goryl et al., 2018).

The presence of βαα steranes in both samples (Fig. 6) indicates significant immaturity (Peters et al., 2005; Bobrovskiy et al., 2018). The C_{29} ααα sterane 20S/(20S + 20R) ratio increases with thermal maturity, reaching 0.5 at equilibrium, with many low maturity samples having ratios of 0.23–0.29 (Seifert et al., 1981). Both samples studied here have ratios <0.23, with a lower ratio for sample 121 (0.14). Similarly the C_{27} αββ/(αββ + ααα) sterane ratio is very low, supporting the same conclusion. The presence of 28,30-DNH can also be an indicator for thermal immaturity, as this compound does not get incorporated into the macromolecular kerogen structure, such that when the thermal maturity level of a given sample increases, the release of hopanes from the kerogen can result in the dilution of 28,30-DNH (Noble et al., 1985). However, the abundance of this compound can be primarily facies controlled in some situations (e.g., Hughes et al., 1985).

There are several maturity parameters determined by the distribution of alkylated isomers of aromatic hydrocarbons, such as DMNs, TMNs and MPs (Alexander et al., 1985; Radke et al., 1986; van Aarssen et al., 1999). The aromatic ratios used in this research are shown in Table 1 and include the methylnaphthalene ratio (MNR) (Radke et al., 1982a), the dimethylnaphthalene ratio (DNR-1) (Alexander et al., 1985), the trimethylnaphthalene ratios (TNR-1; TNR-2; TMNr) (Alexander et al., 1985; Radke et al., 1986), the tetramethylnaphthalene ratio (TeMNr) (van Aarssen et al., 1999), the methylbiphenyl ratio (Alexander et al., 1986), the methylphenanthrene index (MPI) (Radke et al., 1982b), and the methylphenanthrene distribution fraction (Kvalheim et al.,

Table 2
Estimated Vitrinite Reflectance Equivalent (VRE) for selected hydrocarbon maturity parameters.

Parameter	110a (VRE)	121 (VRE)
Ts/(Ts + Tm) hopanes	<0.6%	<0.5%
C_{31} αβ 22S/(22S + 22R) hopanes	<0.5%	<0.5%
C_{32} αβ 22S/(22S + 22R) hopanes	>0.6%	<0.5%
C_{33} αβ 22S/(22S + 22R) hopanes	<0.5%	<0.5%
C_{29} αβ/(αβ + βα) hopanes	<0.6%	<0.6%
C_{30} αβ/(αβ + βα) hopanes	>0.65%	>0.65%
Traces of unstable ββ hopanes	–	<0.4%
C_{29} ααα 20S/(20S + 20R) steranes	0.5%	0.45%
C_{27} αββ/(αββ + ααα) steranes	<0.5%	<0.5%
Presence of unstable βαα steranes	<0.5%	<0.5%
Dimethylnaphthalene ratio-1 (DNR-1)	0.85%	0.8%
Trimethylnaphthalene ratio-2 (TNR-2)	0.65%	0.8%
Trimethylnaphthalene ratio (TMNr)	0.65%	< 0.5%
Methylphenanthrene index (MPI)	0.7%	0.9%

For definitions of parameters see Table 1.

1987). The alkylnaphthalene-derived ratios are generally consistent with the conclusion from the biomarker ratios that sample 121 is less mature than sample 110a (Table 1), except for TNR-2. However, the 3-MBp/2-MBp ratio suggests that sample 121 is more mature than sample 110a, as the isomer with the methyl in the *ortho* position (2-MBp) is less geologically stable than 3-MBp (Cumbers and Alexander, 1987). The ratios derived from the alkylphenanthrene isomers also indicate that sample 121 is more mature. The triaromatic steroid ratio (Mackenzie et al., 1981) indicates that both samples are immature.

The MPI values reported here (Table 1) are inconsistent with the results described above and place these samples with VREs of 0.7–0.9% (Table 2). These MPI values are similar to those reported from some recently fossilised hot springs in the Taupo Volcanic Zone (TVZ) in New Zealand (0.53), and from active hot springs at El Tatio, Chile (0.83) (Teece et al., 2020). The mature component in the Claudia samples implies temperatures of about 120–140 °C, dependent on heating rate and time. Given a typical basin geothermal gradient of 40 °C/km (Sandiford et al., 1998), these values would imply that the compounds are sourced from about 3 km below the surface. However, the geothermal gradient is significantly higher in geothermal fields (Hedenquist, 1986) such that it is more likely that the samples were derived from a much shallower source than indicated by simple burial estimates.

The Late Jurassic deposits from Patagonia were subsequently overlain, but not deeply buried, by Cretaceous and Cenozoic continental and marine successions (Giacosa et al., 2010) and then unearthed with minimal structural disturbance (Guido and Campbell, 2011). This is consistent with the values obtained from the majority of the biomarker ratios and the alkylnaphthalenes, but less consistent with the thermally mature signature derived from the other aromatic parameters and from a few of the biomarkers. This discrepancy may reflect input of hydrocarbons that had been circulated beneath the surface hot spring environment, where the geothermal gradient would be much higher (e.g., Hedenquist, 1986).

Williams et al. (2021) advocated for a facies-oriented understanding of how organic biosignatures are preserved in terrestrial hot springs, in a study examining the polar compounds in both active and recently inactive hot springs in Iceland. The results presented here extend that record back by 150 million years to show that, although the vent site preserves fewer compounds (and in less abundance) than the distal site, saturated compounds can still be preserved in thermally mature sinter.

5.4. Syngeneity of organic matter

GC–MS analyses of the comprehensive cumulative laboratory system blank (basalt sample) detected low amounts of *n*-alkanes, but no aromatic compounds, hopanes or steranes. The *n*-alkanes in the blanks have a different distribution, and subtraction of the blank *n*-alkanes from the *n*-alkanes present in each sample resulted in no differences in the results obtained (Supplementary Fig. S3). In any case, the *n*-alkanes are only used as evidence for the presence of terrigenous input, which is otherwise well supported by the aromatic compounds and steranes present in both samples.

Hydrothermal fluids are known to cause migration of surface and buried organic matter (Reinhardt et al., 2019; Teece et al., 2020). For example, Gonsior et al. (2018) concluded that the chemodiversity in Yellowstone hot springs was inconsistent with limited microbial abundance, and concluded that molecules from deep thermal waters were transported and incorporated into the OM of surface materials. Mixing of OM with different thermal maturities is also evident in each of the samples studied here, with varied thermal maturity signals, and some source indicators showing oxidised terrigenous OM, and others showing hypersaline anoxic OM.

Careful consideration of the different compounds detected, in line with the host rock's geological history, can help distinguish OM sources as well as depositional and post-depositional mechanisms in hot spring sinters. An example of this can be seen in the homohopane ratios in sample 110a of this study, which indicate that inferred maturities vary from <0.5% to >0.6% VRE (Table 2). This result could represent the input of different OM phases, as seen by the varied nature of the clasts that are clearly sourced from different areas within the Claudia vent breccia (e.g., Supplementary Fig. S1d, g).

There are some limitations of this study that should be addressed in future work. Firstly, mainly hydrocarbons were analysed, and it is not known whether functionalised lipids possibly from extant life in the hot spring are present. It is suspected that this was not the case, due to the very low permeabilities of the sinter samples analysed. Secondly, the molecular data within these samples has limited generalisation for regional events due to the small sample suite. Future work should collect samples from across each temperature facies of a well constrained fossilised hot spring to further explore these findings. Thirdly, this study analyses the bulk OM within these samples, which, given the heterogeneity of these samples and the environments from which they are derived, does not provide geospatially resolved data. Future work should examine in situ OM to better extrapolate the various sources and components.

6. Conclusions

This study presents the first documentation of OM contents from ~150 million-year-old siliceous hot spring deposits of the Claudia palaeo-geothermal field in Patagonia, Argentina. A proximal sinter sample (110a) contains a mixture of thermally immature and mature compounds, which suggests the presence of multiple OM sources with variable thermal maturities due to hydrothermal fluid transport, circulation, and/or alteration. In contrast, the distal sinter apron sample (121) retains very immature compounds from terrigenous and microbial OM, which are consistent with no post-depositional thermal heating, whereas some of the aromatic hydrocarbon ratios are indicative of OM that has reached >0.7% VRE (Table 2). The OM contents of both samples include a variety of compounds that have less mature distributions than have been reported even from actively forming hot spring sinters, supporting the interpretation of exceptional preservation in the Claudia geothermal field.

The distal apron area at Claudia presents a unique opportunity to sample pristine biomarker sequences – i.e., a molecular lagerstätten, and a stepping stone into the deep time geological record of geochemical biosignatures in extreme palaeoenvironments – that have been minimally affected by hydrothermal alteration or burial diagenesis. This research provides evidence that ancient hot spring sites can preserve abundant OM, to the same order of abundance (ng HC/g rock) as more recently fossilised sinters from New Zealand and Chile (Teece et al., 2020). However, careful consideration of where sampling should occur within hot springs (i.e. in the distal apron) is needed to increase the likelihood of successful detection of syngeneic OM.

Author contributions

BLT, KAC, MVK and SCG designed the research. KAC and DMG undertook field work. BLT, DMG and AG conducted research. BLT and DMG constructed figures. BLT wrote the initial draft of the paper and managed subsequent versions. DMG, KAC, MVK and SCG provided edits on the manuscript. SCG supervised the research.

Declaration of Competing Interest

The authors declare that they have no known competing financial interests or personal relationships that could have appeared to influence the work reported in this paper.

Data availability

I have uploaded the raw data as a supplementary file

Acknowledgements

We thank Roger Summons for advice in identification of some of the compounds. BLT was funded by an Australian Government Research Training Pathway Scholarship. BLT acknowledges helpful comments that improved this article from the reviewers of her PhD thesis, an anonymous reviewer, and Joe Curiale. Involvement in the project by KAC, MVK and DMG was supported by a research grant from The Royal Society Te Apārangi Marsden Fund, New Zealand. The research for this manuscript took place on the unceded lands of the Bedegal people (UNSW) and the Darug Nation (Macquarie University).

Appendix A. Supplementary material

Supplementary material to this article can be found online at https://doi.org/10.1016/j.orggeochem.2022.104504.

References

Aboglila, S., Grice, K., Trinajstic, K., Snape, C., Williford, K., 2011. The significance of 24-norcholestanes, 4-methylsteranes and dinosteranes in oils and source-rocks from East Sirte Basin (Libya). Applied Geochemistry 26, 1694–1705.
Alexander, R., Kagi, R.I., Rowland, S.J., Sheppard, P.N., Chirila, T.V., 1985. The effects of thermal maturity on distributions of dimethylnaphthalenes and trimethylnaphthalenes in some Ancient sediments and petroleums. Geochimica et Cosmochimica Acta 49, 385–395.
Alexander, R., Cumbers, K., Kagi, R., 1986. Alkylbiphenyls in ancient sediments and petroleums. Organic Geochemistry 10, 841–845.
Alexander, R., Larcher, A.V., Kagi, R.I., Price, P.L., Moldowan, J.M., Albrecht, P., Philp, R.P., 1992. An oil-source correlation study using age-specific plant-derived aromatic biomarkers. In: Biological Markers in Sediments and Petroleum. Prentice Hall, Englewood Cliffs, pp. 201–221.
Allison, P.A., 1988. Konservat-Lagerstätten: cause and classification. Paleobiology 14, 331–344.
Bobrovskiy, I., Hope, J.M., Ivantsov, A., Nettersheim, B.J., Hallmann, C., Brocks, J.J., 2018. Ancient steroids establish the Ediacaran fossil Dickinsonia as one of the earliest animals. Science 361, 1246–1249.
Browne, P., Lawless, J., 2001. Characteristics of hydrothermal eruptions, with examples from New Zealand and elsewhere. Earth-Science Reviews 52, 299–331.
Cady, S.L., Skok, J.R., Gulick, V.G., Berger, J.A., Hinman, N.W., 2018. Siliceous hot spring deposits: why they remain key astrobiological targets. In: From Habitability to Life on Mars. Elsevier, pp. 179–210.
Cady, S., Farmer, J., 1996. In: Fossilization Processes in Siliceous Thermal Springs: Trends in Preservation Along Thermal Gradients. J. Wiley, Chichester, pp. 150–173.
Campbell, K.A., Sannazzaro, K., Rodgers, K.A., Herdianita, N.R., Browne, P.R.L., 2001. Sedimentary facies and mineralogy of the Late Pleistocene Umukuri Silica Sinter, Taupo Volcanic Zone, New Zealand. Journal of Sedimentary Research 71, 727–746.
Campbell, K.A., Lynne, B.Y., Handley, K.M., Jordan, S., Farmer, J.D., Guido, D.M., Foucher, F., Turner, S., Perry, R.S., 2015. Tracing biosignature preservation of geothermally silicified microbial textures into the geological record. Astrobiology 15, 858–882.
Campbell, K.A., Guido, D.M., John, D.A., Vikre, P.G., Rhys, D., Hamilton, A., 2019. The Miocene Atastra Creek sinter (Bodie Hills volcanic field, California and Nevada): 4D evolution of a geomorphically intact siliceous hot spring deposit. Journal of Volcanology and Geothermal Research 370, 65–81.
Campbell, K.A., Nicholson, K., Lynne, B.Y., Browne, P.R.L., 2020. 3D Anatomy of a 60-year-old siliceous hot spring deposit at Hipaua-Waihi-Tokaanu geothermal field, Taupo Volcanic Zone. New Zealand. Sedimentary Geology 402, 105652.
Chaffee, A.L., Johns, R.B., 1983. Polycyclic aromatic hydrocarbons in Australian coals. I. Angularly fused pentacyclic tri- and tetraaromatic components of Victorian brown coal. Geochimica et Cosmochimica Acta 47, 2141–2155.
Chaffee, A.L., Strachan, M.G., Johns, R.B., 1984. Polycyclic aromatic hydrocarbons in Australian coals II. Novel tetracyclic components from Victorian brown coal. Geochimica et Cosmochimica Acta 48, 2037–2043.
Channing, A., Edwards, D., 2009. Silicification of higher plants in geothermally influenced wetlands: Yellowstone as a Lower Devonian Rhynie analog. Palaios 24, 505–521.
Chen, J., Summons, R.E., 2001. Complex patterns of steroidal biomarkers in Tertiary lacustrine sediments of the Biyang Basin, China. Organic Geochemistry 32, 115–126.
Cumbers, K.M., Alexander, R., 1987. Methylbiphenyl, ethylbiphenyl and dimethylbiphenyl isomer distributions in some sediments and crude oils. Geochimica et Cosmochimica Acta 51, 3105–3111.
Didyk, B.M., Simoneit, B.R.T., Brassell, S.C., Eglinton, G., 1978. Organic geochemical indicators of palaeoenvironmental conditions of sedimentation. Nature 272, 216–222.
Djokic, T., Van Kranendonk, M.J., Campbell, K.A., Walter, M.R., Ward, C.R., 2017. Earliest signs of life on land preserved in ca. 3.5 Ga hot spring deposits. Nature Communications 8, 15263.
Djokic, T., Van Kranendonk, M.J., Campbell, K.A., Havig, J.R., Walter, M.R., Guido, D. M., 2021. A reconstructed subaerial hot spring field in the approximately 3.5 Billion-Year-Old Dresser Formation, North Pole Dome, Pilbara Craton. Western Australia. Astrobiology 21, 1–38.
Duda, J.P., Love, G.D., Rogov, V.I., Melnik, D.S., Blumenberg, M., Grazhdankin, D.V., 2020. Understanding the geobiology of the terminal Ediacaran Khatyspyt Lagerstatte (Arctic Siberia, Russia). Geobiology 18, 643–662.
Eglinton, G., Hamilton, R.J., 1967. Leaf epicuticular waxes. Science 156, 1322–1335.
Eickhoff, M., Birgel, D., Talbot, H., Peckmann, J., Kappler, A., 2013. Oxidation of Fe(II) leads to increased C-2 methylation of pentacyclic triterpenoids in the anoxygenic phototrophic bacterium *Rhodopseudomonas palustris* strain TIE-1. Geobiology 11, 268–278.
Fernandez-Turiel, J.L., Garcia-Valles, M., Gimeno-Torrente, D., Saavedra-Alonso, J., Martinez-Manent, S., 2005. The hot spring and geyser sinters of El Tatio, Northern Chile. Sedimentary Geology 180, 125–147.
Gallagher, A., Montanaro, C., Cronin, S., Scott, B., Dingwell, D.B., Scheu, B., 2020. Hydrothermal eruption dynamics reflecting vertical variations in host rock geology and geothermal alteration, Champagne Pool, Wai-o-tapu, New Zealand. Bulletin of Volcanology 82, 1–19.
Giacosa, R., Zubia, M., Sánchez, M., Allard, J., 2010. Meso-Cenozoic tectonics of the southern Patagonian foreland: Structural evolution and implications for Au–Ag veins in the eastern Deseado Region (Santa Cruz, Argentina). Journal of South American Earth Sciences 30, 134–150.
Gonsior, M., Hertkorn, N., Hinman, N., Dvorski, S.E., Harir, M., Cooper, W.J., Schmitt-Kopplin, P., 2018. Yellowstone hot springs are organic chemodiversity hot spots. Scientific Reports 8, 14155.
Goryl, M., Marynowski, L., Brocks, J.J., Bobrovskiy, I., Derkowski, A., 2018. Exceptional preservation of hopanoid and steroid biomarkers in Ediacaran sedimentary rocks of the East European Craton. Precambrian Research 316, 38–47.
Grosjean, E., Love, G.D., Kelly, A.E., Taylor, P.N., Summons, R.E., 2012. Geochemical evidence for an Early Cambrian origin of the 'Q' oils and some condensates from north Oman. Organic Geochemistry 45, 77–90.
Guido, D.M., Campbell, K.A., 2011. Jurassic hot spring deposits of the Deseado Massif (Patagonia, Argentina): Characteristics and controls on regional distribution. Journal of Volcanology and Geothermal Research 203, 35–47.
Guido, D.M., Campbell, K.A., 2014. A large and complete Jurassic geothermal field at Claudia, Deseado Massif, Santa Cruz, Argentina. Journal of Volcanology and Geothermal Research 275, 61–70.
Guido, D.M., Channing, A., Campbell, K.A., Zamuner, A., 2010. Jurassic geothermal landscapes and fossil ecosystems at San Agustín, Patagonia, Argentina. Journal of the Geological Society 167, 11–20.
Guido, D.M., Campbell, K.A., Foucher, F., Westall, F., 2019. Life is everywhere in sinters: examples from Jurassic hot-spring environments of Argentine Patagonia. Geological Magazine 156, 1631–1638.
Guidry, S.A., Chafetz, H.S., 2003. Anatomy of siliceous hot springs: examples from Yellowstone National Park, Wyoming, USA. Sedimentary Geology 157, 71–106.
Hakimi, M.H., Al-Matary, A.M., Ahmed, A.F., 2018. Bulk geochemical characteristics and carbon isotope composition of oils from the Sayhut sub-basin in the Gulf of Aden with emphasis on organic matter input, age and maturity. Egyptian Journal of Petroleum 27, 361–370.
Hamilton, A., Campbell, K., Guido, D., 2019. Atlas of Siliceous Hot Spring Deposits (Sinter) and other Silicified Surface Manifestations in Epithermal Environments. GNS Science report, New Zealand.
Hays, L.E., Graham, H.V., Des Marais, D.J., Hausrath, E.M., Horgan, B., McCollom, T.M., Parenteau, M.N., Potter-McIntyre, S.L., Williams, A.J., Lynch, K.L., 2017. Biosignature preservation and detection in Mars analog environments. Astrobiology 17, 363–400.
Hedenquist, J.W., 1986. Geothermal systems in the Taupo Volcanic Zone: Their characteristics and relation to Volcanism and mineralisation. In: Smith, I.E.M. (Ed.), Late Cenozoic Volcanism in New Zealand. Society of New Zealand Bulletin, pp. 134–168.
Herdianita, N.R., Browne, P.R.L., Rodgers, K.A., Campbell, K.A., 2000. Mineralogical and textural changes accompanying ageing of silica sinter. Mineralium Deposita 35, 48–62.
Holba, A., Dzou, L., Masterson, W., Hughes, W., Huizinga, B., Singletary, M., Moldowan, J., Mello, M., Tegelaar, E., 1998. Application of 24-norcholestanes for constraining source age of petroleum. Organic Geochemistry 29, 1269–1283.
Hoshino, Y., George, S.C., 2015. Cyanobacterial inhabitation on Archean rock surfaces in the Pilbara Craton, Western Australia. Astrobiology 15, 559–574.
Huang, H., Zhang, S., Su, J., 2015. Pyrolytically derived polycyclic aromatic hydrocarbons in marine oils from the Tarim Basin, NW China. Energy & Fuels 29, 5578–5586.
Hughes, W., Holba, A., Miller, D., Richardson, J., 1985. Geochemistry of greater Ekofisk crude oils. In: Thomas, B.M. (Ed.), Petroleum Geochemistry in Exploration of the Norwegian Shelf. Springer, Netherlands, pp. 75–92.
Jiang, Z., Fowler, M.G., 1986. Carotenoid-derived alkanes in oils from northwestern China. Organic Geochemistry 10, 831–839.
Jones, B., Renaut, R.W., 2007. Microstructural changes accompanying the opal-A to opal-CT transition: New evidence from the siliceous sinters of Geysir, Haukadalur, Iceland. Sedimentology 54, 921–948.
Jones, B., Renaut, R.W., 2012. Facies architecture in depositional systems resulting from the interaction of acidic springs, alkaline springs, and acidic lakes: case study of Lake

Roto-a-Tamaheke, Rotorua, New Zealand. Canadian Journal of Earth Sciences 49, 1217–1250.
Jones, B., Renaut, R.W., Rosen, M.R., 1998. Microbial biofacies in hot-spring sinters; a model based on Ohaaki Pool, North Island, New Zealand. Journal of Sedimentary Research 68, 413–434.
Jones, B., Renaut, R.W., Rosen, M.R., 2001. Taphonomy of silicified filamentous microbes in modern geothermal sinters – implications for identification. Palaios 16, 580–592.
Kenig, F., Sinninghe Damsté, J.S., Kock-van Dalen, A.C., Rijpstra, W.I.C., Huc, A.Y., de Leeuw, J.W., 1995. Occurrence and origin of mono-, di-, and trimethylalkanes in modern and Holocene cyanobacterial mats from Abu Dhabi, United Arab Emirates. Geochimica et Cosmochimica Acta 59, 2999–3015.
Kilgour, G., Kennedy, B., Scott, B., Christenson, B., Jolly, A., Asher, C., Rosenberg, M., Saunders, K., 2021. Whakaari/White Island: a review of New Zealand's most active volcano. New Zealand Journal of Geology and Geophysics 64, 273–295.
Killops, S.D., Killops, V.J., 2013. Introduction to Organic Geochemistry. John Wiley & Sons.
Kissin, Y., 1993. Catagenesis of light acyclic isoprenoids in petroleum. Organic Geochemistry 20, 1077–1090.
Kvalheim, O.M., Christy, A.A., Telnæs, N., Bjørseth, A., 1987. Maturity determination of organic matter in coals using the methylphenanthrene distribution. Geochimica et Cosmochimica Acta 51, 1883–1888.
Li, M., Osadetz, K.G., Yao, H., Obermajer, M., Fowler, M.G., Snowdon, L.R., Christensen, R., 1998. Unusual crude oils in the Canadian Williston Basin, southeastern Saskatchewan. Organic Geochemistry 28, 477–488.
Lynne, B.Y., Campbell, K.A., 2003. Diagenetic transformations (opal-A to quartz) of low- and mid-temperature microbial textures in siliceous hot-spring deposits, Taupo Volcanic Zone, New Zealand. Canadian Journal of Earth Sciences 40, 1679–1696.
Lynne, B.Y., Campbell, K.A., Moore, J., Browne, P., 2005. Diagenesis of 1900-year-old siliceous sinter (opal-A to quartz) at Opal Mound, Roosevelt Hot Springs, Utah, USA. Sedimentary Geology 179, 249–278.
Mackenzie, A., Lewis, C., Maxwell, J., 1981. Molecular parameters of maturation in the Toarcian shales, Paris Basin, France—IV. Laboratory thermal alteration studies. Geochimica et Cosmochimica Acta 45, 2369–2376.
Moldowan, J.M., Seifert, W.K., Gallegos, E.J., 1985. Relationship between petroleum composition and depositional environment of petroleum source rocks. American Association of Petroleum Geologists Bulletin 69, 1255–1268.
Montanaro, C., Cronin, S., Scheu, B., Kennedy, B., Scott, B., 2020. Complex crater fields formed by steam-driven eruptions: Lake Okaro, New Zealand. GSA Bulletin 132, 1914–1930.
Noble, R., Alexander, R., Kagi, R.I., 1985. The occurrence of bisnorhopane, trisnorhopane and 25-norhopanes as free hydrocarbons in some Australian shales. Organic Geochemistry 8, 171–176.
Ourisson, G., Albrecht, P., Rohmer, M., 1979. The hopanoids: palaeochemistry and biochemistry of a group of natural products. Pure and Applied Chemistry 51, 709–729.
Owen, R.B., Renaut, R.W., Jones, B., 2008. Geothermal diatoms: a comparative study of floras in hot spring systems of Iceland, New Zealand, and Kenya. Hydrobiologia 610, 175–192.
Peckmann, J., Thiel, V., Reitner, J., Taviani, M., Aharon, P., Michaelis, W., 2004. A microbial mat of a large sulfur bacterium preserved in a Miocene methane-seep limestone. Geomicrobiology Journal 21, 247–255.
Peters, K.E., Walters, C.C., Moldowan, J., 2005. The Biomarker Guide. Cambridge University Press, Cambridge, UK.
Powell, T.G., McKirdy, D.M., 1973. Relationship between ratio of pristane to phytane, crude oil composition and geological environment in Australia. Nature Physical Science 243, 37–39.
Radke, M., Welte, D.H., Willsch, H., 1982a. Geochemical study on a well in the Western Canada Basin: relation of the aromatic distribution pattern to maturity of organic matter. Geochimica et Cosmochimica Acta 46, 1–10.
Radke, M., Willsch, H., Leythaeuser, D., Teichmüller, M., 1982b. Aromatic components of coal: relation of distribution pattern to rank. Geochimica et Cosmochimica Acta 46, 1831–1848.
Radke, M., Welte, D., Willsch, H., 1986. Maturity parameters based on aromatic hydrocarbons: Influence of the organic matter type. Organic Geochemistry 10, 51–63.
Rashby, S.E., Sessions, A.L., Summons, R.E., Newman, D.K., 2007. Biosynthesis of 2-methylbacteriohopanepolyols by an anoxygenic phototroph. Proceedings of the National Academy of Sciences 104, 15099–15104.
Reinhardt, M., Goetz, W., Duda, J.-P., Heim, C., Reitner, J., Thiel, V., 2019. Organic signatures in Pleistocene cherts from Lake Magadi (Kenya) – implications for early Earth hydrothermal deposits. Biogeosciences 16, 2443–2465.
Renaut, R.W., Jones, B., 2011. Hydrothermal Environments, Terrestrial. In: Reitner, J., Thiel, V. (Eds.), Encyclopedia of Geobiology. Springer, Dodrecht, Netherlands.
Robinson, N., Eglinton, G., 1990. Lipid chemistry of Icelandic hot spring microbial mats. Organic Geochemistry 15, 291–298.
Rodgers, K., Browne, P.R.L., Buddle, T.F., Cook, K.L., Greatrex, R.A., Hampton, W.A., Herdianita, N.R., Holland, G.R., Lynne, B.Y., Martin, R., Newton, D., Pastars, D., Sannazarro, K.L., Teece, C.I.A., 2004. Silica phases in sinters and residues from geothermal fields of New Zealand. Earth-Science Reviews 66, 1–61.
Rohmer, M., Bouvier-Nave, P., Ourisson, G., 1984. Distribution of hopanoid triterpenes in prokaryotes. Microbiology 130, 1137–1150.
Romero-Sarmiento, M.-F., Riboulleau, A., Vecoli, M., Versteegh, G.J., 2010. Occurrence of retene in upper Silurian–lower Devonian sediments from North Africa: Origin and implications. Organic Geochemistry 41, 302–306.
Ruff, S.W., Farmer, J.D., 2016. Silica deposits on Mars with features resembling hot spring biosignatures at El Tatio in Chile. Nature Communications 7, 13554.
Ruff, S.W., Campbell, K.A., Van Kranendonk, M.J., Rice, M.S., Farmer, J.D., 2020. The case for ancient hot springs in Gusev Crater, Mars. Astrobiology 20, 475–499.
Sandiford, M., Hand, M., McLaren, S., 1998. High geothermal gradient metamorphism during thermal subsidence. Earth and Planetary Science Letters 163, 149–165.
Schirmer, A., Rude, M.A., Li, X., Popova, E., del Cardayre, S.B., 2010. Microbial biosynthesis of alkanes. Science 329, 559–562.
Schoell, M., McCaffrey, M., Fago, F., Moldowan, J., 1992. Carbon isotopic compositions of 28,30-bisnorhopanes and other biological markers in a Monterey crude oil. Geochimica et Cosmochimica Acta 56, 1391–1399.
Seifert, W.K., Moldowan, J.M., 1978. Applications of steranes, terpanes and monoaromatics to the maturation, migration and source of crude oils. Geochimica et Cosmochimica Acta 42, 77–95.
Seifert, W.K., Moldowan, J.M., 1980. The effect of thermal stress on source-rock quality as measured by hopane stereochemistry. Physics and Chemistry of the Earth 12, 229–237.
Seifert, W.K., Moldowan, J.M., Jones, R., 1981. Application of biological markers in combination with stable carbon isotopes to source rock/oil correlations, Prudhoe Bay, Alaska. American Association of Petroleum Geologists Bulletin 65, 990–991.
Shiea, J., Brassell, S.C., Ward, D.M., 1990. Mid-chain branched mono- and dimethyl alkanes in hot spring cyanobacterial mats: A direct biogenic source for branched alkanes in ancient sediments? Organic Geochemistry 15, 223–231.
Shiea, J., Brassell, S.C., Ward, D.M., 1991. Comparative analysis of extractable lipids in hot spring microbial mats and their component photosynthetic bacteria. Organic Geochemistry 17, 309–319.
Skok, J.R., Mustard, J.F., Ehlmann, B.L., Milliken, R.E., Murchie, S.L., 2010. Silica deposits in the Nili Patera caldera on the Syrtis Major volcanic complex on Mars. Nature Geoscience 3, 838–841.
Squyres, S.W., Arvidson, R.E., Ruff, S., Gellert, R., Morris, R.V., Ming, D.W., Crumpler, L., Farmer, J.D., Des Marais, D.J., Yen, A., McLennan, S.M., Calvin, W., Bell III, J.F., Clark, B.C., Wang, A., McCoy, T.J., Schmidt, M.E., DeSouza Jr, P.A., 2008. Science 320, 1063–1067.
Summons, R.E., Capon, R.J., 1991. Identification and significance of 3β-ethyl steranes in sediments and petroleum. Geochimica et Cosmochimica Acta 55, 2391–2395.
Summons, R.E., Jahnke, L.L., 1990. Identification of the methylhopanes in sediments and petroleum. Geochimica et Cosmochimica Acta 54, 247–251.
Summons, R.E., Jahnke, L.L., 1992. Hopenes and hopanes methylated in ring A: Correlation of the hopanoids from extant methylotrophic bacteria with their fossil analogues. In: Moldowan, J.M., Albrecht, P., Philp, R.P. (Eds.), Biological Markers in Sediments and Petroleum. Prentice Hall, Englewood Cliffs, pp. 182–200.
Summons, R.E., Volkman, J.K., Boreham, C.J., 1987. Dinosterane and other steroidal hydrocarbons of dinoflagellate origin in sediments and petroleum. Geochimica et Cosmochimica Acta 51, 3075–3082.
Summons, R.E., Jahnke, L.L., Hope, J.M., Logan, G.A., 1999. 2-Methylhopanoids as biomarkers for cyanobacterial oxygenic photosynthesis. Nature 400, 554–557.
Teece, B.L., George, S.C., Djokic, T., Campbell, K.A., Ruff, S.W., Van Kranendonk, M.J., 2020. Biomolecules from fossilized hot spring sinters: implications for the search for life on Mars. Astrobiology 20, 537–551.
Trewin, N.H., Bock, G., Goode, J., 1996. In: The Rhynie Cherts: an Early Devonian Ecosystem Preserved by HydroThermal Activity. J. Wiley, Chichester, pp. 131–149.
Trewin, N.H., Fayers, S.R., Kelman, R., 2003. Subaqueous silicification of the contents of small ponds in an Early Devonian hot-spring complex, Rhynie, Scotland. Canadian Journal of Earth Sciences 40, 1697–1712.
van Aarssen, B.G.K., Bastow, T.P., Alexander, R., Kagi, R.I., 1999. Distributions of methylated naphthalenes in crude oils: indicators of maturity, biodegradation and mixing. Organic Geochemistry 30, 1213–1227.
van Aarssen, B.G.K., Alexander, R., Kagi, R.I., 2000. Higher plant biomarkers reflect palaeovegetation changes during Jurassic times. Geochimica et Cosmochimica Acta 64, 1417–1424.
van Kaam-Peters, H.M., Köster, J., van der Gaast, S.J., Dekker, M., de Leeuw, J.W., Sinninghe Damsté, J.S., 1998. The effect of clay minerals on diasterane/sterane ratios. Geochimica et Cosmochimica Acta 62, 2923–2929.
Van Kranendonk, M.J., Baumgartner, R., Djokic, T., Ota, T., Steller, L., Garbe, U., Nakamura, E., 2021. Elements for the origin of life on land: A deep-time perspective from the Pilbara Craton of Western Australia. Astrobiology 21, 39–59.
Volkman, J.K., Farrington, J.W., Gagosian, R.B., 1987. Marine and terrigenous lipids in coastal sediments from the Peru upwelling region at 15°S: Sterols and triterpene alcohols. Organic Geochemistry 11, 463–477.
Volkman, J., Kearney, P., Jeffrey, S., 1990. A new source of 4-methyl sterols and 5α(H)-stanols in sediments: prymnesiophyte microalgae of the genus *Pavlova*. Organic Geochemistry 15, 489–497.
Walter, M.R., 1976. Stromatolites. Elsevier.
Walter, M.R., Des Marais, D.J., 1993. Preservation of biological information in thermal spring deposits: developing a strategy for the search for fossil life on Mars. Icarus 101, 129–143.
Watts-Henwood, N., Campbell, K.A., Lynne, B.Y., Guido, D.M., Rowland, J.V., Browne, P. R., 2017. Snapshot of hot-spring sinter at Geyser Valley, Wairakei, New Zealand, following anthropogenic drawdown of the geothermal reservoir. Geothermics 68, 94–114.
Welander, P.V., Coleman, M.L., Sessions, A.L., Summons, R.E., Newman, D.K., 2010. Identification of a methylase required for 2-methylhopanoid production and implications for the interpretation of sedimentary hopanes. Proceedings of the National Academy of Sciences 107, 8537–8542.
Williams, A.J., Craft, K.L., Millan, M., Johnson, S.S., Knudson, C.A., Juarez Rivera, M., McAdam, A.C., Tobler, D., Skok, J.R., 2021. Fatty acid preservation in modern and

relict hot-spring peposits in Iceland, with implications for organics detection on Mars. Astrobiology 21, 60–82.

Wilmeth, D.T., Myers, K.D., Lalonde, S.V., Mand, K., Konhauser, K.O., Grandin, P., van Zuilen, M.A., 2021. Evaporative silicification in floating microbial mats: patterns of oxygen production and preservation potential in silica-undersaturated streams, El Tatio, Chile. Geobiology. https://doi.org/10.1111/gbi.12476.

Wilmeth, D.T., Nabhan, S., Myers, K.D., Slagter, S., Lalonde, S.V., Sansjofre, P., Homann, M., Konhauser, K.O., Munoz-Saez, C., van Zuilen, M.A., 2020. Depositional evolution of an extinct sinter mound from source to outflow, El Tatio. Chile. Sedimentary Geology 406, 105726.

Withers, N., 1983. Dinoflagellate sterols. Marine Natural Products: Chemical and Biological Perspectives 5, 87–130.

Yunker, M.B., Macdonald, R.W., Vingarzan, R., Mitchell, R.H., Goyette, D., Sylvestre, S., 2002. PAHs in the Fraser River basin: a critical appraisal of PAH ratios as indicators of PAH source and composition. Organic Geochemistry 33, 489–515.

Zakrzewski, A., Kosakowski, P., 2021. Impact of palaeo-wildfires on higher plant parameter revealed by new biomarker indicator. Palaeogeography, Palaeoclimatology, Palaeoecology 579, 110606.

Zakrzewski, A., Kosakowski, P., Waliczek, M., Kowalski, A., 2020. Polycyclic aromatic hydrocarbons in Middle Jurassic sediments of the Polish Basin provide evidence for high-temperature palaeo-wildfires. Organic Geochemistry 145, 104037.

Zundel, M., Rohmer, M., 1985. Hopanoids of the methylotrophic bacteria *Methylococcus capsulatus* and *Methylomonas* sp. as possible precursors of C_{29} and C_{30} hopanoid chemical fossils. FEMS Microbiology Letters 28, 61–64.